

Prepared for *J. Phys. Chem. A*
September 4, 2007

A Diabatic Representation Including Both Valence Nonadiabatic Interactions and Spin-Orbit Effects for Reaction Dynamics

Rosendo Valero and Donald G. Truhlar*

Department of Chemistry and Supercomputing Institute

University of Minnesota, Minneapolis, Minnesota 55455-0431

A diabatic representation is convenient in the study of electronically nonadiabatic chemical reactions because the diabatic energies and couplings are smooth functions of the nuclear coordinates and the couplings are scalar quantities. A method called the fourfold way was devised in our group to generate diabatic representations for spin-free electronic states. One drawback of diabatic states computed from the spin-free Hamiltonian, called a valence diabatic representation, for systems in which spin-orbit coupling cannot be ignored is that the couplings between the states are not zero in asymptotic regions, leading to difficulties in the calculation of reaction probabilities and other properties by semiclassical dynamics methods. Here we report an extension of the fourfold way to construct diabatic representations suitable for spin-coupled systems. In this article we formulate the method for the case of even-electron systems that yield pairs of fragments with doublet spin multiplicity. For this type of system, we introduce the further simplification of calculating the triplet diabatic energies in terms of the singlet diabatic energies via Slater's rules and assuming constant ratios of Coulomb to exchange integrals. Furthermore, the valence diabatic couplings in the triplet manifold are taken equal to the singlet ones. An important feature of the method is the introduction of scaling functions, as they allow one to deal with multibond reactions without having to include

high-energy diabatic states. The global transformation matrix to the new diabatic representation, called the spin-valence diabatic representation, is constructed as the product of channel-specific transformation matrices, each one taken as the product of an asymptotic transformation matrix and a scaling function that depends on ratios of the spin-orbit splitting and the valence splittings. Thus the underlying basis functions are recoupled into suitable diabatic basis functions in a manner that provides a multibond generalization of the switch between Hund's cases in diatomic spectroscopy. The spin-orbit matrix elements in this representation are taken equal to their atomic values times a scaling function that depends on the internuclear distances. The spin-valence diabatic potential energy matrix is suitable for semiclassical dynamics simulations. Diagonalization of this matrix produces the spin-coupled adiabatic energies. For the sake of illustration, diabatic potential energy matrices are constructed along bond-fission coordinates for the HBr and the BrCH₂Cl molecules. Comparison of the spin-coupled adiabatic energies obtained from the spin-valence diabatals with those obtained by *ab initio* calculations with geometry-dependent spin-orbit matrix elements shows that the new method is sufficiently accurate for practical purposes. The method formulated here should be most useful for systems with a large number of atoms, especially heavy atoms, and/or a large number of spin-coupled electronic states.

* Corresponding author. Email: truhlar@umn.edu

1. Introduction

In chemical systems, the interaction between the intrinsic magnetic moments of the electrons and their orbital motion is accounted for by the spin-orbit coupling (SOC) term in the Hamiltonian. The phenomenon of SOC manifests itself clearly in the fine-structure splitting of species in spatially degenerate electronic states, often atoms and diatomic molecules.¹⁻³ Excellent reviews are available on the theory and computation of SOC effects relevant to spectroscopy and chemical reactions.¹⁻⁸ The magnitude of spin-orbit effect increases with the atomic number Z . For relatively light elements, it is a good approximation to introduce SOC in the framework of Russell-Saunders coupling.^{3,9-11} The inclusion of SOC can be important even for elements of the second period. For instance, the 2P state of fluorine is split into the $^2P_{1/2}$ and $^2P_{3/2}$ sublevels, the latter having the lower energy. For many bimolecular reactions at low collision energies, it is a good approximation ($\pm 10\%$ ¹²) to assume that the reagents interact according to the ground-state adiabatic potential energy surface (PES). If the fluorine atom in its $^2P_{3/2}$ sublevel reacts with another species, then SOC increases the reaction barrier height by about $0.4 \text{ kcal mol}^{-1}$ (i.e., one-third of the fluorine spin-orbit splitting),¹³⁻¹⁵ assuming that SOC is completely “quenched” at the transition state. A similar but larger effect occurs for reactions of other halogen atoms.¹⁶ If reaction occurs only on the ground-state surface and nonadiabatic interactions are neglected, then the effect of SOC on thermal rate constants may be approximated as the ratio of transition-state to reactant electronic partition functions.¹⁷ A more complete treatment of SOC involves the inclusion of computed spin-orbit matrix elements, or approximations to them, as functions of the nuclear coordinates, and the construction of the

relevant PESs with SOC included. Examples include $F(^2P) + H_2 \rightarrow HF + H$,¹⁸⁻²¹ $Cl(^2P) + H_2 \rightarrow HCl + H$,^{22,23} or the symmetric $Cl(^2P) + HCl \rightarrow HCl + Cl(^2P)$ reaction.²⁴⁻²⁶

Besides the fine-structure splitting, the second important effect of SOC is that it causes spin-forbidden processes to become partially allowed through interaction and mixing of states of different spin multiplicity.^{8,27-34} The most common occurrence is the interaction between singlet and triplet states, as in the bimolecular $O(^3P, ^1D) + H_2 \rightarrow OH(^2\Pi) + H$ reaction,^{37,38} and in photodissociation of systems such as HCl ,^{39,40} HBr ,⁴¹⁻⁴⁵ CH_3I ,⁴⁶⁻⁵⁰ ICN ,⁵¹⁻⁵⁴ $BrCH_2Cl$,⁵⁵⁻⁵⁸ or $BrCH_2COCl$.⁵⁹⁻⁶⁴ In organic photochemical reactions, the spin-orbit interaction between a triplet state and states of singlet multiplicity promotes decay of the triplet state by phosphorescence and/or intersystem crossing.^{5,6,34}

In order to understand the character of the molecular adiabatic states in the presence of SOC, it is convenient to consider the classic Hund's cases of a diatomic molecule.^{2,3,35} Although Hund's coupling schemes were originally presented primarily to understand the coupling of rotational and electronic angular momenta in rotational spectra,³⁵ it has also been recognized³⁶ that they provide a basis for diabatic representations that can be useful for treating molecular collisions. In the present article we develop this approach in detail for multibond reactions in both molecular collisions and photodissociation.

Each Hund's case corresponds to a different electronic basis set, described by a set of good quantum numbers, that diagonalizes part of the molecular Hamiltonian. Here we will be concerned with the two Hund's cases that do not include nuclear rotational quantum numbers, namely, cases (a) and (c). In Hund's case (a), the basis functions have Λ , Σ , Ω , and S as good quantum numbers and generate a representation that diagonalizes the spin-free electronic Hamiltonian, which may also be called the valence Hamiltonian. Following standard notation,

Λ and Σ are the projections of the spin-free electronic angular momentum and the spin angular momentum S , respectively, on the internuclear axis, and

$$\Omega = \Lambda + \Sigma \quad (1)$$

is the projection of the total electronic angular momentum on the internuclear axis. In Hund's case (c), the basis functions have only Ω as a good quantum number, and in this representation, the sum of the spin-free electronic Hamiltonian and the spin-orbit Hamiltonian is diagonal. The switch between the two cases is controlled by the ratio χ of the spin-orbit coupling to the valence splitting. In particular, Hund's case (c) arises when spin-orbit matrix elements are large relative to the energy splitting of case (a) electronic basis states, whereas Hund's case (a) arises in the opposite limit. Thus, as the internuclear distance decreases, the coupling changes from case (c) to case (a). The change in character of the adiabatic states as a function of χ is an important feature of the adiabatic states that provides some guidance as to how to generate a polyatomic diabatic representation with spin-orbit included, as will be seen below. The ratio χ will serve as a recoupling control parameter and will govern the geometry-dependent character of the generated diabatic basis.

Some of the simplest molecules that manifest SOC are the diatomic hydrides, MH. For these systems, Mulliken found that the spin-orbit constant of atom M varies only slightly when the molecule is formed.^{65,66} For diatomic molecules in which the two atoms have spin-orbit constants of the same order of magnitude, the molecular spin-orbit constant is closer to the mean of the two atomic constants.⁶⁶ These and similar observations motivated the introduction of methods in which the molecular spin-orbit Hamiltonian is written as a sum of effective one-electron one-center operators with empirical atomic spin-orbit constants.^{3,7,71-76} This approximation results in qualitatively or even quantitatively correct spin-orbit matrix elements,

essentially because of the asymptotic r^{-3} dependence of the one-electron term of the spin-orbit operator on the electron-nuclei distances r and the fact that one- and two-electron multicenter terms tend to cancel each other,^{2,70,71} whereas the error committed by neglecting the one-center, two-electron terms is accounted for by the effective operators. Good results have been reported with this method even for systems that show a strong variation of the molecular spin-orbit matrix elements with respect to the nuclear coordinates, such as in the inelastic scattering of oxygen by rare gas atoms.^{71,73,77}

When spin-orbit matrix elements have been computed as a function of nuclear coordinates, it has often been found that they tend to be approximately constant in the entrance arrangement of a bimolecular reaction (or the exit arrangement of a photodissociation reaction), when expressed in a diabatic electronic basis set. This can be understood from the fact that both the diabatic molecular orbitals (MOs) change smoothly and the configuration interaction (CI) coefficients remain essentially constant when the open-shell system with a significant SOC effect is interacting only weakly with the other subsystem.³ For regions of configuration space that show significant variation of the spin-orbit matrix elements, the energies of the spin-free electronic states are often sufficiently separated that the effects of SOC on them are negligible. For example, when expressed in a diabatic basis set, the spin-orbit matrix elements of the $\text{Cl}(^2\text{P}) + \text{H}_2 \rightarrow \text{HCl} + \text{H}$ reaction are almost constant in the entrance valley of the reaction.²³ Although some of the matrix elements do vary significantly in the region of the ground-state barrier, this variation can be safely neglected in this region because the ground-state spin-free surface is well separated from the higher surface there. This is a fairly general phenomenon: that is, the effect of SOC becomes small when an open-shell system interacts strongly with another system not because the spin-orbit matrix elements are quenched by the interaction

(they are not) but rather because the spin-free splittings (which occur in the denominator of a second-order perturbation theory treatment of SOC) become large. A similar explanation in terms of diabatic states was also proposed to rationalize the variation of the spin-orbit matrix elements with the interatomic angle in the $O(^3P, ^1D) + H_2$ system.³⁸

On the basis of these considerations, it seems reasonable to go one step further and assume that the spin-orbit matrix elements are constant, with a numerical value equal to that in the separated-atoms limit. The approximation of assuming the spin-orbit matrix elements are constant in a diabatic basis was compared with the sum-of-one-center-terms spin-orbit Hamiltonian method for the NaCd system.⁷⁸ The former approximation was found to be more accurate in this particular case. The essentially one-center, atomic character of the spin-orbit interaction suggests that an even better starting point would be to work in a valence-bond basis set, as pointed out by Tully.⁷⁹ This so-called ‘atoms-in-molecules’ scheme has been successfully applied to a number of systems involving rare gas and halogen atoms.⁸⁰⁻⁹⁰

In the present study we have chosen to make the approximation of constant spin-orbit matrix elements working in a diabatic representation. Several schemes with varying degrees of generality have been proposed to carry out the adiabatic-to-diabatic transformation, and a large number of references are given in previous papers.^{92,93} Here we will employ a framework for diabatization of spin-free electronic states recently developed in our group and called the fourfold way.⁹²⁻⁹⁴ In general, the diabatic states generated by the fourfold way are linear combinations of more than one valence-bond structure, so one should expect a somewhat larger variation of the spin-orbit matrix elements expressed in the diabatic basis set than for a pure valence-bond treatment. An alternative diabatization method of the direct type (i.e., not requiring nonadiabatic coupling vectors)⁹² when SOC effects are important would be to start

from ‘fully’ adiabatic electronic states, namely, eigenstates of the valence plus spin-orbit Hamiltonian, as done by Morokuma and coworkers for the $\text{CH}_3\text{I} \rightarrow \text{CH}_3 + \text{I}(^2\text{P})$ ⁴⁶⁻⁴⁸ and $\text{ICN} \rightarrow \text{I}(^2\text{P}) + \text{CN}$ ^{51,52} photodissociation systems. This method assumes implicitly that the only coupling between the underlying diabatic states is SOC. However, in general diabatic wave functions interact through both the valence Hamiltonian and the spin-orbit Hamiltonian, and both contributions should be accounted for. This is especially true if the spin-free singlet and/or triplet states show sharp avoided crossings or conical intersections caused by the electronic Hamiltonian.

An example where the dynamics involves valence-state avoided crossings and where spin-orbit coupling in the products is not negligible is the bromoacetyl chloride photodissociation previously studied theoretically by several authors including us.⁵⁹⁻⁶⁴ If we simply add spin-orbit coupling to the spin-free diabatic states that are generated previously,⁶⁴ then we will need a larger basis set, and the states will be coupled even in asymptotic regions. Although quantum mechanical algorithms have been devised to calculate the scattering matrix in the physically meaningful uncoupled representation while carrying out all operations in a coupled diabatic representation (coupled even in the asymptotic region),⁹¹ such a procedure presents unsolved conceptual problems for semiclassical methods that are applicable to larger systems. Since part of the motivation for the present study is to develop a method that can be used to obtain a diabatic representation including SOC for semiclassical calculations on bromoacetyl chloride, we have formulated the new method here for the particular case of photodissociation reactions of even-electron systems that yield pairs of fragments of doublet spin multiplicity, which can only be in singlet and triplet electronic states, one of the fragments in each dissociation channel being an atom with fine-structure splitting. This type of reaction usually starts in a closed-shell

ground electronic state from which the system is promoted by a photon to excited electronic states of dominant singlet character. The photodissociation then leads to pairs of fragments in their ground or excited doublet electronic states.

The purpose of the present study is to provide a simple yet reasonably accurate method to simultaneously include valence nonadiabatic interactions and SOC in the theoretical treatment of chemical reactions, especially photodissociation reactions that start in the singlet manifold. The rest of the paper is organized as follows. Section 2 contains the formulation of the method. In section 2.A the construction of the new diabatic representation for single-channel reactions is illustrated by the case of $\text{HBr} \rightarrow \text{H}(^2\text{S}) + \text{Br}(^2\text{P})$ photodissociation. Section 2.A involves a Hund's case (a) representation at small internuclear distance and a Hund's case (c) representation at large internuclear distance. Section 2.B explains the generalizations of the method that are necessary to treat multichannel reactions, and it may be considered to provide a multibond generalization of Hund's cases (a) and (c). The general method is applied in section 3 to the construction of potential curves suitable for the two-channel $\text{BrCH}_2\text{Cl} \rightarrow \text{Br}(^2\text{P}) + \text{CH}_2\text{Cl}$, $\text{BrCH}_2\text{Cl} \rightarrow \text{CH}_2\text{Br} + \text{Cl}(^2\text{P})$ photodissociation. In this article, a "channel" is a given set of products; this is sometimes called an arrangement or a branching channel in other works. Section 4 contains the conclusions.

2. Formulation of the Method

2.A. Single-Channel Reactions: The HBr Molecule

For even-electron systems that yield pairs of fragments of doublet spin multiplicity, one usually needs to deal only with singlet and triplet electronic states. The construction of a global diabatic representation including spin-orbit coupling starts with the spin-free diabatic potential

matrix formed by a set of singlet and triplet diabatic energies and couplings. In this work we propose a method whereby only the singlet diabatic energies and couplings are computed explicitly, whereas the triplet diabatic energies and couplings are expressed in terms of them. The method is elaborated first for the case of the HBr molecule, although the treatment is also valid for a general diatomic hydride. For HBr, the molecular electronic states considered are those that correlate with $H(^2S) + Br(^2P)$, i.e., with the atoms in their spin-free ground electronic states. When SOC is included, the two dissociation asymptotes are $H(^2S_{1/2}) + Br(^2P_{3/2})$ and $H(^2S_{1/2}) + Br(^2P_{1/2})$, the first being lower in energy. The photodissociation of HBr has been the subject of recent studies as a prototypical process for studying electronically nonadiabatic dynamics in molecules.⁴¹⁻⁴⁵ The equations derived for the HBr molecule can also be applied with a few modifications (see below) to more complicated bond scissions that yield a doublet molecular fragment and a halogen atom.

We will assume from the outset that the *ab initio* valence adiabatic singlet wave functions and energies of the lowest N adiabatic singlet electronic states, that is, the eigenstates of the spin-free electronic Hamiltonian (H^{Val}), have been computed using an electronic structure package. Note that the valence adiabatic states are those that diagonalize H^{Val} , and for shorthand we call them V-adiabatic. These N wave functions and energies are transformed using the fourfold way to the valence diabatic (V-diabatic) states and an $N \times N$ valence diabatic potential matrix containing the V-diabatic energies as diagonal elements and their scalar couplings as nondiagonal elements. When all the electronic states differ by spatial and/or spin symmetry, the V-adiabatic and V-diabatic states are the same. Electronic states that are diabatic with respect to the total electronic Hamiltonian

$$H^{\text{Elec}} = H^{\text{Val}} + H^{\text{SO}}, \quad (2)$$

with H^{SO} being the spin-orbit operator, will be called spin-valence diabatic or fully diabatic and will be denoted F-diabatic. Finally, the eigenstates of H^{Elec} will be termed F-adiabatic states. These representations are summarized in Table 1.

In the method proposed here, the triplet diabatic energies are computed explicitly only at a single nuclear geometry. This single calculation allows one to express the triplet diabatic energies as a function of the singlet diabatic energies by means of Coulomb and exchange integrals,⁹⁵⁻⁹⁷ as detailed below. When not all the diabatic couplings are zero, to complete the construction of the diabatic potential energy matrix the triplet diabatic couplings are assumed equal to the singlet diabatic couplings. This should be a good approximation for open-shell singlets and triplets that distribute themselves into pairs of states with each pair having the same electronic orbital occupancy. In that case, the energies of the singlet and the triplet state in a given pair differ by twice an exchange integral between the open-shell orbitals, and their potential curves or surfaces tend to be parallel to one another. The diabatic energies and couplings (*ab initio* for the singlets and approximate for the triplets) form the spin-free V-diabatic \mathbf{H}^{Val} matrix.

The energies of the singlet and triplet states of a diatomic molecule can be readily expressed in terms of Coulomb and exchange integrals via Slater's rules (or alternatively, Dirac vector rules).⁹⁵⁻⁹⁷ Valence-bond expressions, where the Coulomb and exchange integrals are between atomic orbitals, have been reported for diatomic hydrides,^{97,98} subject to the following assumptions:

- (a) Only the valence atomic orbitals of the halogen atom and the 1s orbital of the hydrogen atom are considered. The closed shells of the halogen atom only contribute a constant term

to the energy of the HX molecule and are therefore neglected. Furthermore, hybridization of the p orbitals is also not treated explicitly.

(b) The relevant electronic configurations are only the covalent ones. Ionic configurations, and configurations in which electrons of the X atom are excited, are neglected.

(c) All atomic orbitals are assumed orthogonal. Although this is a rather strong approximation, it is justified by the success of semiempirical models such as the well-known London-Eyring-Polanyi-Sato (LEPS)⁹⁹ and extended LEPS¹⁰⁰ models.

(d) The Coulomb and exchange integrals are assumed to be the same for all the electronic states.

With these assumptions, the two doublet electronic states of the H and Br atoms generate two singlet and two triplet V-adiabatic states for the HBr molecule, and these can be written as^{97,98}

$$E(^1\Sigma) = 4Q_{H\pi} + Q_{H\sigma} + J_{H\sigma} - 2J_{H\pi}, \quad (3a)$$

$$E(^3\Sigma) = 4Q_{H\pi} + Q_{H\sigma} - J_{H\sigma} - 2J_{H\pi}, \quad (3b)$$

$$E(^1\Pi) = 3Q_{H\pi} + 2Q_{H\sigma} - J_{H\sigma}, \quad (3c)$$

$$E(^3\Pi) = 3Q_{H\pi} + 2Q_{H\sigma} - J_{H\sigma} - 2J_{H\pi}. \quad (3d)$$

In these expressions, $Q_{H\sigma}$ and $Q_{H\pi}$ are Coulomb integrals, and $J_{H\sigma}$ and $J_{H\pi}$ are exchange integrals between hydrogen and halogen atomic orbitals. In particular, H denotes the $1s$ orbital of the hydrogen atom, and σ , π denote the $4p$ bromine orbitals. These states are also V-diabatic because their spatial symmetry is different within each spin manifold, and states with different spin multiplicity cannot interact through H^{Val} . Hereafter, we will refer to these electronic states as V-diabatic.

Subsequently, our aim is to construct V-diabatic triplet potential curves as functions of the computed V-diabatic singlet potential curves. There are four unknowns in eqs 3a–3d (the Coulomb and exchange integrals), whereas only $E(^1\Sigma)$ and $E(^1\Pi)$ are assumed known. Therefore, two additional equations are required. We have adopted the constant-Coulomb-ratio approximation used by Eyring and Polanyi¹⁰¹ in their well-known^{102,103} semiempirical model of chemical reactions; in the present case it involves assuming a constant ratio between the Coulomb integrals and the total interaction energy between the electrons in the two atomic orbitals H and σ or H and π . The approximation was formulated for the case that each orbital is occupied by one electron and the electrons are coupled to a bound singlet state¹⁰²

$$Q_{H\sigma}/(Q_{H\sigma} + J_{H\sigma}) = A_1, \quad (4a)$$

$$Q_{H\pi}/(Q_{H\pi} + J_{H\pi}) = A_2. \quad (4b)$$

For simplicity, we will use the following equivalent equations instead of eqs 4a and 4b:

$$Q_{H\sigma}/J_{H\sigma} = C_1, \quad (5a)$$

$$Q_{H\pi}/J_{H\pi} = C_2. \quad (5b)$$

The constants C_1 and C_2 can be determined from the energies of the four V-diabatic states at a given geometry. Hence, from a single computation of the triplet energies at this geometry it is possible to derive the whole set of approximate triplet potential curves. For the particular choice of the ground-state equilibrium distance R_e , the equations to be solved are:

$$E(^1\Sigma; R_e) = (4C_2 - 2) J_{H\pi}(R_e) + (C_1 + 1) J_{H\sigma}(R_e), \quad (6a)$$

$$E(^3\Sigma; R_e) = (4C_2 - 2) J_{H\pi}(R_e) + (C_1 - 1) J_{H\sigma}(R_e), \quad (6b)$$

$$E(^1\Pi; R_e) = 3C_2 J_{H\pi}(R_e) + (2C_1 - 1) J_{H\sigma}(R_e), \quad (6c)$$

$$E(^3\Pi; R_e) = (3C_2 - 2)J_{H\pi}(R_e) + (2C_1 + 1)J_{H\sigma}(R_e), \quad (6d)$$

from which the constants are obtained as

$$C_1 = \frac{E(^1\Sigma, R_e) + 2E(^1\Pi, R_e) - 7E(^3\Sigma, R_e) + 6E(^3\Pi, R_e)}{5(E(^1\Sigma, R_e) - E(^3\Sigma, R_e))}, \quad (7a)$$

$$C_2 = \frac{E(^1\Sigma, R_e) + 2E(^1\Pi, R_e) + 3E(^3\Sigma, R_e) - 4E(^3\Pi, R_e)}{5(E(^1\Pi, R_e) - E(^3\Pi, R_e))}. \quad (7b)$$

Once the constants are known, we can express the potential energy curves of the triplet v-diabatic states as functions of the potential curves of the v-diabatic singlet states. Using eqs 6a–d one can derive the relations

$$E(^3\Sigma) = E(^1\Sigma) - 2J_{H\sigma}, \quad (8a)$$

$$E(^3\Pi) = E(^1\Pi) - 2J_{H\pi}. \quad (8b)$$

Finally, the exchange integrals $J_{H\sigma}, J_{H\pi}$ must be expressed as functions of $E(^1\Sigma), E(^1\Pi), C_1,$ and C_2 . This can be done by using eqs 6a and 6c but for a generic internuclear distance instead of the ground-state equilibrium distance:

$$J_{H\sigma}(R) = \frac{3C_2 E(^1\Sigma, R) - (4C_2 - 2)E(^1\Pi, R)}{3C_2(1 + C_1) - (2C_1 - 1)(4C_2 - 2)}, \quad (9a)$$

$$J_{H\pi}(R) = \frac{(1 + C_1)E(^1\Pi, R) - (2C_1 - 1)E(^1\Sigma, R)}{3C_2(1 + C_1) - (2C_1 - 1)(4C_2 - 2)}. \quad (9b)$$

In case some of the singlet diabatic couplings are not zero, the triplet diabatic couplings would be assumed equal to the open-shell singlet couplings of same electronic configuration, but we will not need this until section 2.B. The diabatic energies and couplings can then be used to set up the v-diabatic matrix. This completes the construction of the v-diabatic potential energy curves for the HBr molecule, or for a halogen bond in a polyatomic molecule, if only

singlet and triplet states are considered. Similar expressions to those in eqs 3–9 can be derived for electronic states of other spin multiplicity.⁹⁷

The construction of a consistent F-diabatic representation for a single-channel process such as $\text{HBr} \rightarrow \text{H}(^2\text{S}) + \text{Br}(^2\text{P})$ is, in principle, straightforward, and will be discussed next. Note that the discussion is general in that it does not involve the assumptions of eqs 5a and 5b. It can be used either with the treatment of eqs 3–9 or with *ab initio* calculations of the triplet potential curves.

For systems of the type $\text{HBr} \rightarrow \text{H}(^2\text{S}) + \text{Br}(^2\text{P})$, the usual strategy for constructing a representation that is F-diabatic,^{21,25,104-109} and the one we have adopted here, is to carry out a similarity transformation of the V-diabatic matrix by means of the matrix that diagonalizes the representation of H^{SO} in the V-diabatic basis in the dissociation limit. In general, a transformation of the V-diabatic basis would make \mathbf{H}^{Val} nondiagonal. But a key point in this case is that the transformation only mixes eigenvectors of \mathbf{H}^{Val} that are degenerate at $R = \infty$, and it leaves \mathbf{H}^{Val} diagonal. Furthermore it diagonalizes the matrix of the spin-orbit operator in the V-diabatic basis, $\mathbf{H}^{\text{SO,Val}}$, at $R = \infty$. The final F-diabatic matrix is obtained by adding the diagonal (in the new representation) SOC matrix to the similarity-transformed matrix representing \mathbf{H}^{Val} . For HBr, there are 12 V-diabatic states, one arising from the spin-free $^1\Sigma$ state, two from the $^1\Pi$ state, three from the $^3\Sigma$ state, and six from the $^3\Pi$ state. Thus, the matrices of H^{Val} and H^{SO} (and therefore H^{Elec}) in the V-diabatic basis set are of order 12. The transformation matrix to the F-diabatic representation, here denoted $\mathbf{C}^{(n)}$, with $n = 12$, satisfies¹⁰⁹

$$\mathbf{C}^{(n)\dagger} \mathbf{H}^{\text{SO,Val}}(\infty) \mathbf{C}^{(n)} = \mathbf{H}^{\text{SO,F}}(\infty). \quad (10)$$

where the elements of $\mathbf{H}^{\text{SO,Val}}(\infty)$ are

$$\mathbf{H}_{\alpha\alpha'}^{\text{SO,Val}}(\infty) = \langle \alpha | H^{\text{SO}} | \alpha' \rangle. \quad (11)$$

The elements of $\mathbf{H}^{\text{SO,Val}}(\infty)$ are presented in Table 2, and the elements of $\mathbf{C}^{(n)}$ are presented in Table 3. The spin basis set for the singlet v-diabatic states contains a single function (for S and M_S equal to zero), whereas the three spin functions for the triplet v-diabatic states ($S = 1$) were chosen as the function with M_S equal to zero plus linear combinations of the functions with M_S equal to 1 and -1, as follows:

$$|1+\rangle \equiv \frac{1}{\sqrt{2}} (|S=1, M_S=1\rangle + |S=1, M_S=-1\rangle), \quad (12a)$$

$$|1-\rangle \equiv \frac{1}{\sqrt{2}} (|S=1, M_S=1\rangle - |S=1, M_S=-1\rangle). \quad (12b)$$

The elements of the diagonal matrix on the right-hand side of eq 10 are the eigenvalues of $\mathbf{H}^{\text{SO,Val}}(\infty)$, i.e., the elements of H^{SO} in the F-diabatic representation,

$$(\mathbf{H}^{\text{SO,F}}(\infty))_{\beta\beta'} = \langle \beta | H^{\text{SO}} | \beta' \rangle \delta_{\beta\beta'}, \quad (13)$$

where $\beta \equiv j_A \Omega_A$ and $j_{MB} \Omega_{MB}$ represents the n different combinations of the atomic and molecular fragment $j_a \Omega$ substates, where j_a is the total electronic angular momentum. Thus, from eq 10 one can see that $\mathbf{C}^{(n)}$ is a unitary matrix with the eigenvectors of $\mathbf{H}^{\text{SO,Val}}$ as its columns. Finally, the F-diabatic potential matrix $\mathbf{H}^{\text{F}}(R)$ is constructed as

$$\mathbf{H}^{\text{F}}(R) = \mathbf{C}^{(n)\dagger} \mathbf{H}^{\text{Val}}(R) \mathbf{C}^{(n)} + \mathbf{H}^{\text{SO,F}}(\infty). \quad (14)$$

The elements of the H^{Val} matrix at $R = \infty$ are

$$\mathbf{H}_{\alpha\alpha'}^{\text{Val}}(\infty) = E_{\alpha}(\infty)\delta_{\alpha\alpha'}, \quad (15)$$

where $E_{\alpha}(\infty)$ is the energy of the n degenerate V-diabatic states, labeled by “ α ”, in this dissociation limit. Diagonalization of the real symmetric F-diabatic matrix $\mathbf{H}^{\text{F}}(R)$ at the set of internuclear distances of interest yields the F-adiabatic potential energy curves.

The calculations presented here for HBr are only intended to illustrate the method for single-channel reactions. For that reason, relatively low-level electronic structure methods and basis sets have been employed. The V-adiabatic singlet and triplet states of the HBr molecule (which are also V-diabatic, see above) and the spin-orbit matrix elements, have been calculated using the MOLPRO program.¹¹⁰ The state-averaged complete-active-space self-consistent field (SA-CASSCF) method^{111,112} has been used with an active space containing six electrons in four active molecular orbitals (five electrons from the three $4p$ orbitals of bromine and one electron from the $1s$ orbital of hydrogen). The method is here denoted SA-CASSCF(6,4). The two singlet states ($^1\Sigma$ and $^1\Pi$) and the two triplet states ($^3\Sigma$ and $^3\Pi$) derived from $\text{H}(^2\text{S}) + \text{Br}(^2\text{P})$ have been included in the average with equal weights of 0.25 each. Basis sets of the segmented type have been used, as required¹¹³ by the spin-orbit code implemented in MOLPRO. The standard 6-311G basis set,¹¹⁴ and the Binning-Curtiss VTZP basis set,¹¹⁵ have been utilized for hydrogen and bromine, respectively. The H^{SO} operator is defined as the full spin-orbit part of the Breit-Pauli operator.¹¹³ The adiabatic potential curves with spin-orbit included are obtained by diagonalization of the matrix of H^{Elec} of eq 2 in a basis of eigenstates of H^{Val} (in the present simple case the V-diabats and the V-adiabats are the same).¹¹³

The spin-orbit splitting of the bromine atom, $\Delta E_{\text{SO,Br}}$, obtained here at the SA-CASSCF(6,4) level (3397 cm^{-1} or 0.42 eV), is in reasonable agreement with (288 cm^{-1} lower than) the experimental value (3685 cm^{-1} or 0.46 eV).¹¹⁶ For comparison, note that in benchmark basis-set-limit configuration interaction with single and double excitations (CISD) calculations the spin-orbit splitting of Br was found to be only 100 cm^{-1} lower than the experiment.¹¹⁷

Figure 1 presents the V -diabatic potential energy curves for HBr. In this and in subsequent figures, the zero of energy has been defined as the spin-free asymptotic energy. The classification of the states follows the labeling $^{2S+1}\Lambda^{\pm}$, where “ \pm ” refers to the even/odd symmetry of the $\Lambda = 0$ electronic wave functions with respect to the operator of reflection on a plane that contains the internuclear axis. The matrix of the total electronic Hamiltonian in the basis of the 12 V -diabatic substates is nondiagonal due to H^{SO} . The eight F-adiabatic potential energy curves obtained by diagonalization of \mathbf{H}^{Elec} are presented in Figure 2. The energy of the $\text{H}(^2\text{S}) + \text{Br}(^2\text{P}_{3/2})$ level is $-\frac{\Delta E_{\text{SO,Br}}}{3}$, and the energy of the $\text{H}(^2\text{S}) + \text{Br}(^2\text{P}_{1/2})$ level is $\frac{2\Delta E_{\text{SO,Br}}}{3}$. In the dissociation limit, the eight F-adiabatic states that correlate with j_{Br} equal to $\frac{3}{2}$ are $X\ ^1\Sigma_{0+}$, $A\ ^1\Pi_1$ (two substates), $a\ ^3\Pi_1$ (two substates), $a\ ^3\Pi_2$ (two substates), and $a\ ^3\Pi_{0-}$. The four F-adiabatic states that correlate with j_{Br} equal to $\frac{1}{2}$ are $t\ ^3\Sigma_1$ (two substates), $a\ ^3\Pi_{0+}$, and $t\ ^3\Sigma_{0-}$. The molecular terms are labeled with a mixed Hund’s case (a)/case (c) notation according to $^{2S+1}\Lambda_{|\Omega|^{\pm}}$,⁴⁵ where

$$|\Omega| \equiv |\Lambda + \Sigma|. \quad (16)$$

The $^{2S+1}\Lambda$ label refers to the Hund's case (a) basis state with the largest coefficient in the Hund's case (c) wave function at short internuclear distances. The states with $|\Omega| \neq 0$ are doubly degenerate and the states with $|\Omega|$ equal to zero are further classified according to the parity (+ or -) of their wave function.

One of the assumptions of our method is that the molecular SOC matrix elements can be taken as the atomic bromine matrix elements. To substantiate this assumption, Figure 3 presents the dependence of the five unique spin-orbit matrix elements in the V-diabatic basis as a function of internuclear distance. The Ω values of the coupled substates are also specified in the labels (note the $\Delta\Omega = 0$ selection rule for SOC).^{1,3} As observed in the figure, the percent change of the spin-orbit matrix elements with respect to their asymptotic value does not exceed about 10%, except for $\langle {}^3\Pi_0 | H^{\text{SO}} | {}^1\Sigma_0^+ \rangle$, which shows a large decrease at short internuclear distances. The energy splitting between the spin-free potential curves at R equal to or less than 2.0 Å is large enough (especially between the ${}^1\Sigma^+$ and ${}^3\Pi$ states, Figure 1) that the variation in the spin-orbit matrix elements should not produce significant changes in the energy of the F-adiabatic states due to SOC. Qualitatively, this argument can be understood from the second-order perturbation theory expression of the energy of the F-adiabatic state I , derived from SOC of the V-diabatic I substate to the other V-diabatic substates, denoted J :

$$E_I^F = E_I^{\text{Val}} + \langle I | H^{\text{SO}} | I \rangle + \sum_{I \neq J} \frac{|\langle I | H^{\text{SO}} | J \rangle|^2}{E_I^{\text{Val}} - E_J^{\text{Val}}}. \quad (17)$$

In this equation, E_I^{Val} is the spin-free energy of the V-diabatic substate I , and the next two terms are the first-order and second-order contributions to SOC for that substate. Thus, for

sufficiently large energy separation between the spin-free electronic states (that is, for a sufficiently short H-Br internuclear distance), the effect of their mutual SOC through the second-order term in eq 17 on the energies of the F-adiabatic states becomes negligible. However, for degenerate states with $S \neq 0$, the first-order term is nonzero. Thus, the ${}^3\Pi$ state generates four potential curves with different values of Ω , and these curves are split even at short internuclear distances (see Figure 2). Even in this case, the percentage error on the energies of the F-adiabatic ${}^3\Pi_{0^\pm,1,2}$ states incurred from the assumption that the diagonal $\langle {}^3\Pi_i | H^{\text{SO}} | {}^3\Pi_i \rangle$ matrix elements are equal to their atomic values is very small. The accuracy of the constant SOC scheme has been tested by comparing with *ab initio* F-adiabatic energies. The mean unsigned error (MUE) in the energies of the potential curves has been calculated for each electronic state, including only internuclear distances less or equal than 5.0 Å (the shortest distance for which the splitting between the electronic states becomes negligible) and larger or equal than the H-Br equilibrium distance (about 1.45 Å). The MUEs vary between 0.6 meV for the ${}^1\Sigma_{0^+}$ state and 3.2 meV for the ${}^3\Pi_{0^-}$ state. These small errors can be considered satisfactory.

The construction of an approximate F-diabatic representation in the present treatment involves the calculation of approximate triplet V-diabatic potential curves as a function of the computed singlet v-diabatic curves. Figure 4 shows the triplet potential curves obtained with the method proposed here and the corresponding *ab initio* curves for comparison. The curves derived from computing the constant ratios defined in eqs 5a and 5b at the equilibrium distance of the ground state (Figure 4a) are most accurate at intermediate and short R distances. In contrast, if the constants are determined at a longer R distance as in the results presented in

Figure 4b, the long-range region of the potential is well reproduced but the accuracy deteriorates at shorter distances. The difference between the approximate V-diabatic triplet states and the *ab initio* (SA-CASSCF(6,4)) ones is zero when R is 1.45 Å (Figure 4a) or 2.0 Å (Figure 4b). This is the expected result, as the model is exact for the distances at which the constants in eqs 5a and 5b are determined. The MUEs of the model potential curves in Figure 4a are calculated as explained above, and they are 0.17 and 0.05 eV for $^3\Sigma^+$ and $^3\Pi$, respectively. The maximum errors are 0.38 eV (1.8 Å) and 0.12 eV (1.7 Å), respectively, at the internuclear distances indicated in parentheses. For the curves in Figure 4b, the MUEs are 0.35 and 0.15 eV and the maximum errors are 1.35 eV (1.45 Å) and 0.65 eV (1.45 Å). We have chosen the more accurate (on the average) triplet potential curves of Figure 4a to construct the F-diabatic representation.

The F-diabatic matrix containing *ab initio* singlet diabatic energies and model triplet diabatic energies (the diabatic couplings are all zero) has been diagonalized to generate F-adiabatic potential energy curves for HBr, which are presented in Figure 5. Comparing Figure 5 with the SA-CASSCF(6,4) F-adiabatic potential curves shown in Figure 2, one can observe deviations mainly in the spin-orbit states having a large contribution from the $^3\Sigma^+$ V-diabatic state. The MUEs of the different F-adiabatic potential curves with respect to the *ab initio* curves are 0.001, 0.028, 0.046, 0.052, 0.067, 0.15, 0.15 and 0.051 eV for the $^1\Sigma_{0+}$, $^1\Pi_1$, $^3\Pi_1$, $^3\Pi_2$, $^3\Pi_{0-}$, $^3\Sigma_1$, $^3\Sigma_{0-}$, and $^3\Pi_{0+}$ electronic states, respectively. The maximum errors are 0.003 (2.8 Å), 0.081 (2.4 Å), 0.11 (1.7 Å), 0.12 (1.7 Å), 0.12 (1.8 Å), 0.37 (1.8 Å), 0.38 (1.8 Å), and 0.12 eV (1.7 Å), respectively, for the internuclear distances indicated in parentheses. The MUEs and maximum errors follow closely those of the model triplet curves

(see above). We deem these results sufficiently accurate for practical purposes, especially given the limited accuracy of *ab initio* electronic structure calculations for larger systems for which the method should be most useful.

2.B. Multichannel Reactions

Several extensions of the method presented in section 2.A for single-channel reactions are necessary for multichannel reactions. Here, by multichannel reactions we mean reactions with more than one dissociative arrangement, each with one or more atoms or molecular fragments having SOC. The first extension is necessary because there are several possible reasons why the transformation matrices to F-diabatic representations suitable for each dissociation channel are different for the different channels. Most simply, this arises when the electronic states of the species that experience SOC are different in different channels, because then the transformation matrices are necessarily different. Another, less obvious reason for the transformation matrices to differ is when the correlation of the diabatic states with the electronic states of the fragments is different in different dissociation channels, even if the electronic states of the species with fine-structure splitting are the same in all dissociation channels. In either case, the solution we put forward is to construct a global transformation matrix as the product of two or more channel-specific transformation matrices (constructed as a generalization of the method in section 2.A, with the generalization explained below), in such a way that the global F-diabatic representation is continuous and correct fine-structure splittings are obtained in all dissociation limits.

A second improvement to the single-channel method required for multichannel reactions concerns the construction of a diagonal SOC matrix in the F-diabatic representation. Thus,

unless the species with fine-structure splitting are identical in all dissociation channels (e.g., for the $\text{Cl}(^2\text{P}) + \text{HCl} \rightarrow \text{HCl} + \text{Cl}(^2\text{P})$ reaction^{24,25}), the elements of the SOC matrix will be different in different channels. As a consequence, the SOC matrix elements for one channel must be transformed smoothly into those for the other channels as the system evolves along the reaction coordinate from one dissociation limit through the strong-interaction region and to other dissociation limits. Otherwise, the SOC matrix elements arising from the fine-structure splitting in one dissociation limit would unphysically influence the fine-structure splittings in the other dissociation limits.

We should emphasize that the new diabaticization method presented here is designed for multichannel singlet photodissociation reactions and is not, in general, well suited to studying phenomena such as the heavy-atom singlet-triplet coupling effects usually observed in organic spectroscopy and photochemistry,^{8,31,32,34} because of the need of damping both the transformation matrices and the SOC elements at short internuclear distances. However, many aspects of the new method are more general, and, with proper calibration of the damping functions, the new method could be used to study the effect of a single heavy atom singlet-triplet coupling, provided the SOC matrix elements do not show a large conformational dependence.

The underlying reason why these extensions to the single-channel method must be introduced is that the set of adiabatic states correlating with the different fragment states is in general not large enough to guarantee that all the electronic configurations are represented in all dissociation channels. That means that in many cases, the diabatic electronic states change their character gradually along the reaction coordinate, and the parentage of some or all of the diabatic states is lost. To illustrate the general situation, we will consider the case of a molecule

AMB with two atoms, A and B , that can be released at relatively low energies, M being an atomic or molecular fragment. An example could be $AMB = \text{BrCH}_2\text{Cl}$, with $A = \text{Br}$ and $B = \text{Cl}$. We want to study the dissociation processes $AMB \rightarrow A + MB$ and $AMB \rightarrow AM + B$, where the AMB molecule can be in any of the electronic states that correlate with the electronic configurations of the fragments in the energy range of interest. We will assume that the simultaneous scission of the two bonds, i.e., the $AMB \rightarrow A + M + B$ process, is not feasible in the energy range studied. We will also assume that AM and MB can be in two non-degenerate electronic states with the same spin multiplicity, whereas A and B are in a single spin-coupled degenerate energy level with nonzero total spin. Since the fourfold way method transforms N adiabatic states into a diabatic potential matrix with N diabatic energies along the diagonal, all of the diabatic states that correlate with the $A + MB$ channel also correlate with $AM + B$.

Hereafter, the electronic manifolds stemming from a given dissociation channel will be denoted $C\Gamma-k$, where Γ and k are integers referring to the channel and to the electronic manifold within a given channel, respectively. In the $A + MB$ and $AM + B$ dissociation limits, the electronic manifolds are grouped into sets of degenerate states, due to the degeneracy of the A and B atomic electronic states. For the AMB system, the channel definitions are as follows:

$$A + MB(\text{gr}): C1-1, \quad (18a)$$

$$A + MB(\text{exc}): C1-2, \quad (18b)$$

$$AM(\text{gr}) + B: C2-1, \quad (18c)$$

$$AM(\text{exc}) + B: C2-2, \quad (18d)$$

where ‘gr’ and ‘exc’ stand for the ground and first excited electronic states of the molecular fragments. An example of C2-1 would be $\text{BrCH}_2 + \text{Cl}(^2\text{P})$, and an example of C2-2 would be

$\text{BrCH}_2^* + \text{Cl}(^2\text{P})$, where an asterisk denotes an electronically excited state. Similarly C1-1 would be $\text{Br}(^2\text{P}) + \text{CH}_2\text{Cl}$ and so forth.

The first issue one faces for multichannel reactions is that, in general, the transformation matrices to F-diabatic representations suitable for each dissociation channel are different for the different channels, as explained above. The approach that we have adopted to define a global transformation matrix to an F-diabatic representation is as follows. In the simplest case, in the dissociation limits both atom A and B are in the same n -fold degenerate electronic state; thus, in that case the C1-1, C1-2, C2-1, and C2-2 manifolds are each composed of n degenerate states. Then, one can construct an $N \times N$ transformation matrix \mathbf{C} corresponding to the $A + MB$ channel, with $N = 2n$, from the $n \times n$ transformation matrix $\mathbf{C}^{(n)}$ corresponding to each of C1-1 and C1-2. Analogously, the $N \times N$ transformation matrix \mathbf{D} corresponding to the $AM + B$ channel can be constructed from the $n \times n$ transformation matrix $\mathbf{D}^{(n)}$ corresponding to each of C2-1 and C2-2. Recall that in the particular case of the single-channel, single-electronic manifold $\text{HBr} \rightarrow \text{H}(^2\text{S}) + \text{Br}(^2\text{P})$ dissociation the value of n was 12. The $\mathbf{H}^{\text{SO,Val}}(\infty)$ and $\mathbf{H}^{\text{Val}}(\infty)$ matrices of eqs 11 and 15, respectively, are now $N \times N$ diagonal matrices. In the dissociation limit, the spin-orbit operator couples separately the electronic states in the C1-1 manifold and those in the C1-2 manifold. Therefore, the $\mathbf{H}_{\text{Cl}}^{\text{SO,Val}}(\infty)$ matrix has the structure

$$\mathbf{H}_{\text{Cl}}^{\text{SO,Val}}(\infty) = \begin{pmatrix} \mathbf{H}_{\text{Cl-1}}^{\text{SO,Val}} & \mathbf{0}^{(n)} \\ \mathbf{0}^{(n)} & \mathbf{H}_{\text{Cl-2}}^{\text{SO,Val}} \end{pmatrix}, \quad (19)$$

where $\mathbf{H}_{\text{C1-1}}^{\text{SO,Val}}$ and $\mathbf{H}_{\text{C1-2}}^{\text{SO,Val}}$ are $n \times n$ spin-orbit matrices analogous to $\mathbf{H}^{\text{SO,Val}}(\infty)$ in eq 11 and $\mathbf{0}^{(n)}$ is an $n \times n$ block of zeroes. The transformation matrix \mathbf{C} has an analogous structure to $\mathbf{H}_{\text{C1}}^{\text{SO,Val}}(\infty)$

$$\mathbf{C} = \begin{pmatrix} \mathbf{C}^{(n)} & \mathbf{0}^{(n)} \\ \mathbf{0}^{(n)} & \mathbf{C}^{(n)} \end{pmatrix}. \quad (20)$$

The form of eqs 19 and 20 assumes that the V-diabatic states are ordered such that the first n V-diabatic states belong to the C1-1 manifold, and the V-diabatic states $n + 1$ to $2n$ are the ones that belong to the C1-2 manifold. Once this choice is made, the form of the \mathbf{D} matrix can be deduced from the form of the \mathbf{C} matrix based on the correlations of the V-diabatic states with the states in the C2-1 and C2-2 manifolds. For example, let us assume that the V-diabatic states 1 to k in C1-1 correlate with states 1 to k in C2-1; states $k + 1$ to n in C1-1 correlate with states $k + 1$ to n in C2-2; states $n + 1$ to $n + k + 1$ in C1-2 correlate with states $n + 1$ to $n + k + 1$ in C2-2; and states $n + k + 2$ to $2n$ in C1-2 correlate with states $n + k + 2$ to $2n$ in C2-1. In this case, the structure of the \mathbf{D} matrix would be

$$\mathbf{D} = \begin{pmatrix} \mathbf{C}_{1-k}^{(n)} & \mathbf{0}_{1-k}^{(n)} \\ \mathbf{0}_{(k+1)-n}^{(n)} & \mathbf{C}_{(k+1)-n}^{(n)} \\ \mathbf{0}_{1-k}^{(n)} & \mathbf{C}_{1-k}^{(n)} \\ \mathbf{C}_{(k+1)-n}^{(n)} & \mathbf{0}_{(k+1)-n}^{(n)} \end{pmatrix}, \quad (21)$$

where $\mathbf{C}_{1-k}^{(n)}$ represents rows 1 to k of the $\mathbf{C}^{(n)}$ matrix, with an analogous meaning for the rest of the symbols.

Once the channel-specific \mathbf{C} and \mathbf{D} matrices are defined, it is necessary to construct a global F-diabatic representation, taking those matrices as the starting point. As explained in the Introduction, the appropriate basis set in the dissociation limits, where the splitting between the

spin-free electronic states is zero and the effect of SOC is maximal, is that of Hund's case (c). For short internuclear distances, when the splitting between the spin-free states is large, the effect of SOC is minimal and the F-adiabatic states are essentially Hund's case (a) states. In this situation, one can define new matrices for the $A + MB$ and $AM + B$ channels, here denoted \mathbf{C}^{Dyn} and \mathbf{D}^{Dyn} , respectively. (The superscript "dyn" stands for "dynamical", meaning that these matrices generate a representation suitable for reaction dynamics.)

We impose the conditions that the new matrices \mathbf{C}^{Dyn} and \mathbf{D}^{Dyn} be equal to \mathbf{C} and \mathbf{D} in the dissociation limits (where Hund's case (c) is appropriate) and be equal to the unit matrix at short $A-M$ or $M-B$ internuclear distances (where Hund's case (a) is a more suitable representation), respectively. Besides, the new matrices \mathbf{C}^{Dyn} and \mathbf{D}^{Dyn} must be unitary at all internuclear distances. A convenient way to fulfill all these conditions is to construct a Cayley parametrization of \mathbf{C}^{Dyn} and \mathbf{D}^{Dyn} , in which these matrices are expressed in terms of Hermitian matrices, \mathbf{X}^{Dyn} and \mathbf{Y}^{Dyn} :

$$\mathbf{C}^{\text{Dyn}} = (\mathbf{I} - i\mathbf{X}^{\text{Dyn}})(\mathbf{I} + i\mathbf{X}^{\text{Dyn}})^{-1}, \quad (22)$$

$$\mathbf{D}^{\text{Dyn}} = (\mathbf{I} - i\mathbf{Y}^{\text{Dyn}})(\mathbf{I} + i\mathbf{Y}^{\text{Dyn}})^{-1}, \quad (23)$$

where \mathbf{I} is the unit matrix and i denotes $\sqrt{-1}$. Note that the two factors in each of eqs 22 and 23 commute, giving two equivalent definitions of the parametrization of \mathbf{C}^{Dyn} and \mathbf{D}^{Dyn} . In these equations, \mathbf{X}^{Dyn} and \mathbf{Y}^{Dyn} are defined in terms of the matrices, \mathbf{X}^{∞} and \mathbf{Y}^{∞} , obtained at the dissociation limits for the $A + MB$ and the $AM + B$ channel, respectively, by inverting the Cayley parametrizations of \mathbf{C} and \mathbf{D} , i.e.,

$$\mathbf{X}^{\infty} = i(\mathbf{C} + \mathbf{I})^{-1}(\mathbf{C} - \mathbf{I}), \quad (24)$$

$$\mathbf{Y}^{\infty} = i(\mathbf{D} + \mathbf{I})^{-1}(\mathbf{D} - \mathbf{I}), \quad (25)$$

times a scaling function, f_{bond} , where “bond” is the bond broken in each dissociation channel

$$\mathbf{X}^{\text{Dyn}} = f_{A-M} \mathbf{X}^{\infty}, \quad (26)$$

$$\mathbf{Y}^{\text{Dyn}} = f_{M-B} \mathbf{Y}^{\infty}. \quad (27)$$

The scaling functions for the $A + MB$ and $AM + B$ channels are defined as

$$f_{A-M} = \frac{(\tanh(C_{A-M} (\chi_{A-M} - \chi_{0,A-M})) + 1)}{2}, \quad (28)$$

$$f_{M-B} = \frac{(\tanh(C_{M-B} (\chi_{M-B} - \chi_{0,M-B})) + 1)}{2}, \quad (29)$$

where C_{A-M} , C_{M-B} , $\chi_{0,A-M}$ and $\chi_{0,M-B}$ are dimensionless parameters and χ_{A-M} and χ_{M-B} are recoupling control parameters (see introduction) defined as

$$\chi_{A-M} = \frac{\Delta E_{\text{SO},A} \Delta E_{\text{Val},B}}{(\Delta E_{\text{Val},A})^2}, \quad (30)$$

$$\chi_{M-B} = \frac{\Delta E_{\text{SO},B} \Delta E_{\text{Val},A}}{(\Delta E_{\text{Val},B})^2}. \quad (31)$$

In these equations, $\Delta E_{\text{SO},A}$ is the fine-structure splitting of atom A , $\Delta E_{\text{SO},B}$ is the fine-structure splitting of atom B , and $\Delta E_{\text{Val}, A-M}$ and $\Delta E_{\text{Val}, M-B}$ are the splittings between the most repulsive and the most attractive v-diabatic states along the $A-M$ and $M-B$ dissociation coordinates, respectively. A key assumption in the present scheme is that the scaling functions are smooth and slowly varying so that they do not generate nonadiabatic coupling.

Finally, the global transformation matrix \mathbf{T}^{Dyn} to the global F-diabatic representation is constructed as the matrix product of \mathbf{C}^{Dyn} and \mathbf{D}^{Dyn} :

$$\mathbf{T}^{\text{Dyn}} = \mathbf{C}^{\text{Dyn}} \mathbf{D}^{\text{Dyn}}. \quad (32)$$

That is, for a given set of nuclear coordinates, the global F-diabatic matrix, \mathbf{H}^{F} , is constructed as

$$\mathbf{H}^{\text{F}}(R) = \mathbf{T}^{\text{Dyn}\dagger} \mathbf{H}^{\text{Val}}(R) \mathbf{T}^{\text{Dyn}} + \mathbf{H}^{\text{SO,F}}(R). \quad (33)$$

In this equation, $\mathbf{H}^{\text{Val}}(R)$ is the $N \times N$ matrix that contains the v-diabatic energies and couplings, and $\mathbf{H}^{\text{SO,F}}(R)$, that will now be defined, is the global diagonal $N \times N$ spin-orbit matrix for the AMB system in the F-diabatic representation. Note that whereas for the HBr molecule $\mathbf{H}^{\text{SO,F}}$ is always equal to its value in the dissociation limit (see eq 14), here $\mathbf{H}^{\text{SO,F}}$ is distance-dependent. As explained above, in the F-diabatic representation the diagonal elements of the SOC matrix for atom A need to be transformed to those of the SOC matrix for atom B along any reaction pathway that connects the $A + MB$ channel with the $AM + B$ channel. To this aim, we have defined a symmetric scaling function of the form

$$\beta(m, \Delta) = \frac{\beta_A (R_{A-M} - R_{e,A-M} + \Delta)^m + \beta_B (R_{M-B} - R_{e,M-B} + \Delta)^m}{(R_{A-M} - R_{e,A-M} + \Delta)^m + (R_{M-B} - R_{e,M-B} + \Delta)^m}, \quad (34)$$

where β_A and β_B are certain fractions that depend on the atomic electronic states of the fine-structure splittings of atoms A and B , respectively. $R_{e,A-M}$ and $R_{e,M-B}$ are the equilibrium distances of bonds $A-M$ and $M-B$, respectively, in the ground state of the AMB molecule, m is an integer power, and Δ is a parameter that smoothes out the transition from β_A to β_B in the region where R_{A-M} and R_{M-B} are close to $R_{e,A-M}$ and $R_{e,M-B}$ and prevent the factors from becoming negative for odd m values (provided R_{A-M} and R_{M-B} are not too small).

Henceforth, we will define the energy of the lowest spin-free asymptotic level as the zero of energy. Following this convention, let us assume that atoms A and B both have two fine-structure levels that have the same values of the atomic total electronic angular momentum j_a , i.e., j_L for the lower fine-structure level and j_H for the higher fine-structure level. Furthermore, from the n total substates, the lower fine-structure level contains s degenerate substates and the higher fine-structure level contains r degenerate substates. Then, in eq 34, β_A and β_B are equal to $-\Delta E_{SO,A} \frac{r}{n}$ and $-\Delta E_{SO,B} \frac{r}{n}$, respectively, for the lower fine-structure level and are equal to $\Delta E_{SO,A} \frac{s}{n}$ and $\Delta E_{SO,B} \frac{s}{n}$, respectively, for the higher fine-structure level. Let us denote the function in eq 34 as $\beta(m,\Delta)_L$ in the first case and as $\beta(m,\Delta)_H$ for the second case. The elements of the $\mathbf{H}^{\text{SO,F}}$ matrix are

$$(\mathbf{H}^{\text{SO,F}})_{\alpha\alpha'} \delta_{\alpha\alpha'} = \beta(m,\Delta)_L, \quad (35)$$

where $1 \leq \alpha, \alpha' \leq s$ denote substates belonging to the lower fine-structure level, and

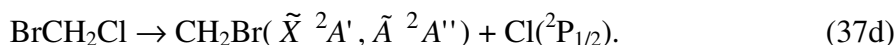
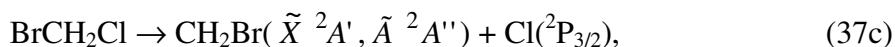
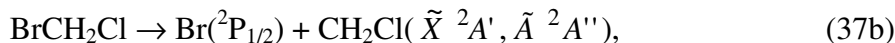
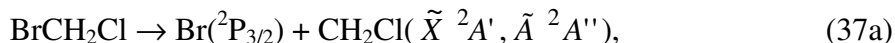
$$(\mathbf{H}^{\text{SO,F}})_{\alpha\alpha'} \delta_{\alpha\alpha'} = \beta(m,\Delta)_H, \quad (36)$$

where $1 \leq \alpha, \alpha' \leq r$ denote substates belonging to the higher fine-structure level. In the general case, that is, when the fine-structure levels in each channel differ in number, in their sets of j_a values, or in both, care should be exercised to insert appropriate β_A and β_B values in eq 34 and to establish the correlations between the V-diabatic states in the $A + MB$ and the $AM + B$ channels. One example is the $\text{O}(^3\text{P}, ^1\text{D}) + \text{H}_2 \rightarrow \text{OH}(^2\Pi) + \text{H}$ reaction, where there are three fine-structure levels in reactants (corresponding to $j_{\text{O}(^3\text{P})}$ equal to 0, 1, and 2) and two fine-structure levels in products (for $j_{\text{OH}(^2\Pi)}$ equal to $\frac{1}{2}$ and $\frac{3}{2}$). In this case, it should be possible

to construct a reasonable F-diabatic representation by correlating some of the electronic states of reactants with some of the products, because not all of the states are relevant to the non-adiabatic reaction dynamics.^{37,38} The transformation matrices would have a more complicated structure than the one shown in eqs 20 and 21. Similar changes should be introduced for the treatment of other systems of this more general type.

3. Application to the Two-Channel BrCH₂Cl System

Chlorobromomethane (BrCH₂Cl) is one of the species responsible for the destruction of atmospheric ozone, and the mechanism of its photodissociation has been the subject of recent theoretical scrutiny.⁵⁵⁻⁵⁸ Photodissociation of the BrCH₂Cl molecule proceeds along the following reaction pathways:



Equations 37a-37d represent two channels (Br(²P) + CH₂Cl and CH₂Br + Cl(²P)) and eight separate electronic dissociation limits, with the CH₂Br and CH₂Cl radicals in their ground or first excited electronic state, and with the halogen atoms in their $j = \frac{1}{2}$ or $\frac{3}{2}$ fine-structure levels.

The SA-CASSCF method has been employed to compute the energies of the six lowest singlet V-adiabatic states as functions of the C-Br and C-Cl dissociation coordinates, with an active space of twelve electrons in the following eight molecular orbitals: $\sigma(\text{C-Br})$, $\sigma^*(\text{C-Br})$,

$\sigma(\text{C-Cl})$, $\sigma^*(\text{C-Cl})$, $n(\text{Cl})$, $n'(\text{Cl})$, $n(\text{Br})$ and $n'(\text{Br})$. The method is here denoted SA-CASSCF(12,8). The notations $n(\text{X})$ and $n'(\text{X})$ refer to nonbonding p -type orbitals centered on the halogen atoms. The same active space has been used to compute the six lowest triplet v -adiabatic states at the SA-CASCI level in a basis formed from the singlet v -adiabatic MOs. The SOC matrix elements have been computed in the basis of these v -adiabatic singlet and triplet states using the GAMESS¹¹⁸ electronic structure package. The 6-31G(d,p) Gaussian basis set¹¹⁹ was used for all these calculations with five spherical harmonic d functions for nonhydrogenic atoms. The equilibrium ground-state geometry of the BrCH_2Cl molecule has been computed separately at the MP2(FC)/6-311+G(d,p) level using Gaussian03.¹²⁰ The parameters obtained are $R(\text{C-Br}) = 1.934 \text{ \AA}$, $R(\text{C-Cl}) = 1.763 \text{ \AA}$, $R(\text{H-C}) = 1.086 \text{ \AA}$, $\angle\text{Cl-C-Br} = 113.5^\circ$, $\angle\text{H-C-Cl} = 108.9^\circ$, and $\angle\text{H-C-Cl-Br} = 119.4^\circ$. Simple bond-scission potential energy curves have been constructed by stretching the C-Br bond or the C-Cl bond keeping the rest of parameters fixed at the ground-state equilibrium geometry. The molecule always keeps C_s symmetry, but no symmetry restrictions were applied to the MOs in the SA-CASSCF and SA-CASCI calculations.

The twenty-four different F-adiabatic potential curves and their asymptotic correlations are shown in Figure 6. Each of the two doublet electronic states of CH_2Br or CH_2Cl combines with the six spin-orbit substates of the chlorine and the bromine atom, respectively, to yield a total of 12 substates. The lowest eight substates correspond to the halogen atoms in their $^2P_{3/2}$ state and the highest four to the $^2P_{1/2}$ state. The zero of energy has been defined as the energy of the lowest spin-free asymptotic limit, in this case, $\text{Br}(^2P) + \text{CH}_2\text{Cl}(\tilde{X} \ ^2A')$. Therefore, the energy of the $\text{Br}(^2P_{3/2}) + \text{CH}_2\text{Cl}(\tilde{X} \ ^2A')$ level is $-\frac{\Delta E_{\text{SO,Br}}}{3}$, and the energy of the $\text{Br}(^2P_{1/2}) +$

$\text{CH}_2\text{Cl}(\tilde{X}^2A')$ level is $\frac{2\Delta E_{\text{SO,Br}}}{3}$. The spin-orbit splitting, $\Delta E_{\text{SO,Br}}$, obtained for bromine is 3212 cm^{-1} (0.40 eV), compared with an experimental value of 3685 cm^{-1} (0.46 eV).¹¹⁶ The theoretical value is less accurate than the one obtained above for the HBr molecule (0.42 eV), due to the different basis sets used, namely, a Binning-Curtiss VTZP basis set with 49 contracted Gaussian functions for bromine in the HBr molecule and a 6-31G(d,p) basis set with 28 contracted Gaussian functions for bromine in the BrCH_2Cl molecule. The theoretical spin-orbit splitting of chlorine, $\Delta E_{\text{SO,Cl}}$, is 843 cm^{-1} (0.105 eV) versus an experimental value of 881 cm^{-1} (0.11 eV).¹¹⁶ Although the theoretical values are not particularly accurate, a distinct advantage of the method proposed here over direct computation of SOC matrix elements is that experimental values could be used to construct the F-diabatic representation.

The V-diabatic potential energy matrix for the singlet states was obtained using the fourfold way⁹²⁻⁹⁴ as implemented in HONDOPLUS, version 5.1.¹²¹ The triplet V-diabatic potential matrix was also computed by the fourfold way for comparison with the one constructed with the approximate expressions in eqs 3–9. The fourfold way has been explained in detail before,⁹²⁻⁹⁴ and only a brief account is given here. The method is based on the construction of diabatic MOs (DMOs) to guarantee configurational uniformity along nuclear-coordinate paths. The construction of the DMOs proceeds by maximization of a certain functional (D_3) that is a linear combination of two one-electron density matrices and one transition density matrix; this is called the threefold density criterion. In some cases, an additional term must be defined in order to guarantee smoothness of the DMOs, and the method is called the fourfold way. The new term contains an overlap-like quantity of the MOs with a set of so-called reference MOs. The fourfold way DMOs are used to construct groups of orthonormal diabatic configuration state functions (DCSFs), each group spanning a characteristic subspace that defines a diabatic

state determined by configurational uniformity. Finally, the adiabatic many-electron wave functions are expressed in terms of the DCSFs, with the CI coefficients of the expansion being used to define the adiabatic-to-diabatic transformation matrix.

In the application of the fourfold-way diabatization method to the BrCH_2Cl system, it was found that configurational uniformity was not well fulfilled when the threefold density criterion⁹² was applied separately along the C-Cl and C-Br stretching coordinates. To solve this problem, the more general fourfold way was employed. A prerequisite to introduce the reference DMOs of the fourfold way is to choose a standard orientation for the molecule. Here, the molecule has been situated with the two halogen atoms and the carbon atom in the xz plane. The Br atom is at the coordinate origin, the C-Br bond points in the positive direction of the z axis, and the Cl atom has a positive value of x . Two orbitals per halogen atom for a total of four reference DMOs are required to ensure a consistent set of DCSFs. The reference DMOs are chosen in a specific molecular orientation (here denoted by primed coordinates), and for a general molecular geometry they must be transformed to the standard orientation (unprimed). The specific orientation for the Br atom coincides with the standard orientation, since the Br atom is located at the coordinate origin. The specific orientation for the Cl atom is defined with the x' axis parallel to the C-Cl bond and with the $x'z'$ plane being the Cl,C,Br plane. Finally, the y' axis is orthogonal to the $x'z'$ plane. The four reference DMOs are the DMOs representing the nonbonding p orbitals in the specific orientation, that is, the, $\text{Cl}(p_{y'})$, $\text{Cl}(p_{z'})$, $\text{Br}(p_{x'})$ and $\text{Br}(p_{y'})$ orbitals. To have reference DMOs that are geometry-independent, the reference DMOs are computed by the threefold way at a geometry where the molecule is in its specific orientation and the C-Cl and C-Br bond lengths are stretched one at a time to 5.0 Å. The coefficients of the $p_{y'}$ - and $p_{z'}$ -type atomic orbitals of chlorine and those of the $p_{x'}$ - and $p_{y'}$ -

type atomic orbitals of bromine thus obtained define the reference DMOs. To compute the potential energy curves, the reference DMOs are transformed from the specific to the standard orientation by means of the rotation matrix that relates the two coordinate systems.

To simplify the application of the fourfold way to BrCH_2Cl , only the V -adiabatic states showing avoided crossings along the reaction coordinate have been included in the diabaticization procedure, leaving out those adiabatic states that are separated from the rest in the strong-interaction region. For the singlet manifold, the ground $^1\Sigma$ state and the higher (sixth) V -adiabatic SA-CASSCF states have been excluded from the diabaticization procedure, and the remaining four V -adiabatic states have been included in the fourfold way. For the triplet manifold, out of the six SA-CASCI states the highest (sixth) V -adiabatic state is not included in the diabaticization. Although they should strictly be taken into account, the couplings between the $^3\Sigma$ state, which is the counterpart of the bonding $^1\Sigma$ state, and the other states will be ignored. The DCSFs obtained for the four singlet states, and for the four triplet V -diabatic states excluding the $^3\Sigma$ state and the highest (sixth) state, and their distribution into diabatic groups, are presented in Table 4. The singlet and the triplet states are composed of the same DCSFs, the only difference being the spin coupling of the open-shell electrons. As can be seen, the DCSFs represent mainly excitations from the nonbonding orbitals of the halogens to the antibonding C-Br and C-Cl σ^* orbitals. The dominant DCSFs for the different diabatic groups (states) in Table 4 along the C-Br and the C-Cl scission coordinates are as follows, starting from the $\text{Br}(^2\text{P}) + \text{CH}_2\text{Cl}(\tilde{X} \ ^2A')$ asymptote: s_1 and t_2 change from χ_1 (C-Br) to χ_2 (C-Cl) and χ_3 ($\text{CH}_2\text{Br}(\tilde{A} \ ^2A'') + \text{Cl}(^2\text{P})$ asymptote); s_2 and t_3 change from χ_4 (C-Br) to χ_5 (C-Cl) and χ_6 ($\text{CH}_2\text{Br}(\tilde{A} \ ^2A'') + \text{Cl}(^2\text{P})$ asymptote). Starting now from the $\text{CH}_2\text{Br}(\tilde{X} \ ^2A') + \text{Cl}(^2\text{P})$

asymptote, s_3 and t_4 change from χ_8 (C-Cl) to χ_7 (C-Br) and χ_9 ($\text{Br}(^2\text{P}) + \text{CH}_2\text{Cl}(\tilde{A}^2A'')$ asymptote); and s_4 and t_5 change from χ_{11} (C-Cl) to χ_{10} (C-Br) and χ_{12} ($\text{Br}(^2\text{P}) + \text{CH}_2\text{Cl}(\tilde{A}^2A'')$ asymptote). The four V-diabatic singlet states obtained with the fourfold way along with the two V-adiabatic singlet states, which are assumed V-diabatic, are shown in Figure 7.

The triplet V-diabatic states can be constructed from the singlet V-diabatic states using the formulas in eqs 5-9, as was done for the HBr diatomic, and can also be computed by the fourfold way from the *ab initio* V-adiabatic triplet states. The difference in the application of eqs 5-9 to a nonlinear molecule such as BrCH_2Cl , with respect to the application to a linear molecule such as HBr, is that for BrCH_2Cl , which in this study keeps C_s symmetry, the two components of each $^1\Pi$ electronic state (which can be called $^1\Pi_a$ and $^1\Pi_b$) have slightly different energies. When the energies of the $^1\Sigma$ and $^1\Pi_a$ states are used in the formulas, one obtains energies for the $^3\Sigma$ state and for one of the components of the $^3\Pi$ state. Likewise, using the energies of the $^1\Sigma$ and $^1\Pi_b$ states, one obtains energies for the $^3\Sigma$ state and for the second component of the $^3\Pi$ state. Since the energies of the $^1\Pi_a$ and $^1\Pi_b$ states differ, different energies are also obtained for the $^3\Sigma$ state in these two instances. We have defined the energy of the $^3\Sigma$ state produced by the method as the average of the two energies thus obtained. Figure 8 compares the triplet V-diabatic potential curves obtained from the singlets by means of eqs 5-9 with those obtained from the *ab initio* triplet V-adiabatic curves using the fourfold way. The agreement between the *ab initio* triplet potential curves in Figure 8a and the curves in Figure 8b is excellent for the states that correlate with the CH_2Br and CH_2Cl fragments in their ground electronic state. Although the agreement is only qualitative for the triplet states that correlate

with the molecular fragments in their excited states, we consider it is good enough for our purposes. This comparison is a validation, within the accuracy with which Figure 8b agrees with Figure 8a, of the simplification of obtaining the triplet diabats from the singlet ones.

The triplet diabatic couplings that are computed from the *ab initio* V-adiabatic triplet states using the fourfold way are compared with the singlet couplings in Figure 9. The couplings between states 1 and 3 and between states 2 and 4 are the only nonzero couplings involving states 2-5 because in C_s symmetry the diabatic states are classified as $s_1, t_2 (A'')$; $s_2, t_3 (A')$; $s_3, t_4 (A'')$; and $s_4, t_5 (A')$. As observed in the figure, the agreement between the singlet and triplet diabatic couplings is excellent and justifies the approximation of taking the triplet couplings equal to the singlet couplings for the electronic states of open-shell character.

The V-diabatic matrix for the BrCH_2Cl system, constructed from the diabatic energies and couplings just presented, must be transformed to a global F-diabatic matrix using eq 33. The transformation matrix \mathbf{C}^{Dyn} for the $\text{Br}(^2\text{P}) + \text{CH}_2\text{Cl}$ channel used to construct \mathbf{T}^{Dyn} (see eq 32) derives from the asymptotic \mathbf{C} matrix as shown in eqs 22, 24, 26, 28 and 30. The scaling function for \mathbf{C} was defined in eq 28 for the prototype AMB system; for the BrCH_2Cl system, the parameters were chosen after some trial and error as $C_{C-Br} = 12$ and $\chi_{0,C-Br} = 0.2$. These parameters ensure that the F-diabatic potential energy matrices generated by \mathbf{C}^{Dyn} as this matrix varies from the \mathbf{C} matrix at the $\text{Br}(^2\text{P}) + \text{CH}_2\text{Cl}$ asymptotic limit to the unit matrix at short C-Br distances have a smooth dependence on the C-Br distance. The parameters in eq 30 are defined as follows: $\Delta E_{\text{SO,Br}} = 0.3982$ eV is the (constant) fine-structure splitting of the bromine atom, $\Delta E_{\text{Val,C-Br}}$ is the difference between the energies of the s_1 and s_0 V-diabatic

potential curves (Figure 7), and $\Delta E_{\text{val},C-Cl}$ is the difference between the energies of the s_3 and s_0 V-diabatic potential curves.

The elements of the $\mathbf{C}^{(n)}$ matrix, constructed from the 12×12 total electronic Hamiltonian of the V-diabatic states that correlate with either one of $\text{Br}(^2\text{P}) + \text{CH}_2\text{Cl}(\tilde{X} \ ^2A')$ or $\text{Br}(^2\text{P}) + \text{CH}_2\text{Cl}(\tilde{A} \ ^2A'')$ are presented in Table 3. The structure of the \mathbf{C} matrix is (see eq 20):

$$\mathbf{C} = \begin{pmatrix} \mathbf{C}^{(n)} & \mathbf{0}^{(n)} \\ \mathbf{0}^{(n)} & \mathbf{C}^{(n)} \end{pmatrix}. \quad (38)$$

The asymptotic transformation matrix \mathbf{D} for the $\text{CH}_2\text{Br} + \text{Cl}(^2\text{P})$ channel can be constructed from the \mathbf{C} matrix according to the correlations of the singlet and triplet diabatic states with the electronic states of $\text{Br}(^2\text{P}) + \text{CH}_2\text{Cl}$ and $\text{CH}_2\text{Br} + \text{Cl}(^2\text{P})$ shown in Figures 7 and 8. In the $\text{Br}(^2\text{P}) + \text{CH}_2\text{Cl}$ dissociation limit, the singlet V-diabatic states are divided into two groups of degenerate states as $(s_0, s_1, s_2, t_1, t_1', t_1'', t_2, t_2', t_2'', t_3, t_3', t_3'')$ and $(s_3, s_4, s_5, t_4, t_4', t_4'', t_5, t_5', t_5'', t_6, t_6', t_6'')$. Notice that each V-diabatic triplet potential curve in Figure 8 corresponds to three states with M_S equal to $0, \pm 1$; e.g., the (t_1, t_2, t_3) curves give rise to the $t_1, t_1', t_1'', t_2, t_2', t_2'', t_3, t_3', t_3''$ states. The structure of the \mathbf{D} matrix is

$$\mathbf{D} = \begin{pmatrix} \mathbf{C}_1^{(n)} & \mathbf{0}_1 \\ \mathbf{0}_{2-4} & \mathbf{C}_{2-4}^{(n)} \\ \mathbf{C}_5^{(n)} & \mathbf{0}_5 \\ \mathbf{0}_{6-7} & \mathbf{C}_{6-7}^{(n)} \\ \mathbf{C}_8^{(n)} & \mathbf{0}_8 \\ \mathbf{0}_9 & \mathbf{C}_9^{(n)} \\ \mathbf{C}_{10}^{(n)} & \mathbf{0}_{10} \\ \mathbf{0}_{11-12} & \mathbf{C}_{11-12}^{(n)} \\ \mathbf{0}_{13} & \mathbf{C}_{13}^{(n)} \\ \mathbf{C}_{14-16}^{(n)} & \mathbf{0}_{14-16} \\ \mathbf{0}_{17} & \mathbf{C}_{17}^{(n)} \\ \mathbf{C}_{18-19}^{(n)} & \mathbf{0}_{18-19} \\ \mathbf{0}_{20} & \mathbf{C}_{20}^{(n)} \\ \mathbf{C}_{21}^{(n)} & \mathbf{0}_{21} \\ \mathbf{0}_{22} & \mathbf{C}_{22}^{(n)} \\ \mathbf{C}_{23-24}^{(n)} & \mathbf{0}_{23-24} \end{pmatrix}, \quad (39)$$

where, for instance, $\mathbf{C}_{2-4}^{(n)}$ represents rows 2 to 4 of the $\mathbf{C}^{(n)}$ matrix, with an analogous meaning for the rest of the symbols. The form of eq 39 can be understood from the V-diabatic state correlations with $\text{CH}_2\text{Br}(\tilde{X}^2A') + \text{Cl}(^2P)$ and $\text{CH}_2\text{Br}(\tilde{A}^2A'') + \text{Cl}(^2P)$, which are:

- s_0 and t_1, t_1', t_1'' correlate with $\text{CH}_2\text{Br}(\tilde{X}^2A') + \text{Cl}(^2P)$;
- s_1, s_2 and $t_2, t_2', t_2'', t_3, t_3', t_3''$ correlate with $\text{CH}_2\text{Br}(\tilde{A}^2A'') + \text{Cl}(^2P)$;
- s_3, s_4 , and $t_4, t_4', t_4'', t_5, t_5', t_5''$ correlate with $\text{CH}_2\text{Br}(\tilde{X}^2A') + \text{Cl}(^2P)$;
- s_5 and t_6, t_6', t_6'' correlate with $\text{CH}_2\text{Br}(\tilde{A}^2A'') + \text{Cl}(^2P)$.

The transformation matrix \mathbf{D}^{Dyn} used along with \mathbf{C}^{Dyn} to generate the global F-diabatic representation is constructed from \mathbf{D} as shown in eqs 23, 25 27, 29 and 31. The parameters in eq 29 in the particular case of $\text{CH}_2\text{Br} + \text{Cl}(^2P)$ are $C_{C-Cl} = 200$ and $\chi_{0,C-Cl} = 0.022$. In eq 31,

$\Delta E_{\text{SO,Cl}} = 0.1045$ eV is the (constant) fine-structure splitting of the chlorine atom, and the other parameters have the same meaning as for the \mathbf{C}^{Dyn} matrix. Note that considerable care was taken when choosing the $f_{\text{C-Cl}}$ function in eq 29 as well as the $\chi_{\text{C-Cl}}$ function in eq 31. The reason is that the \mathbf{D} matrix is not block-diagonal, as seen in eq 39. Thus, $f_{\text{C-Cl}}$ needs to be defined in such a way that it is only significantly different from zero or one in a limited region, close to the C-Cl equilibrium distance. In this region the V-diabatic states are close in energy, and the mixing of the states that come from $\text{CH}_2\text{Br}(\tilde{X}^2A') + \text{Cl}(^2P)$ with those that come from $\text{CH}_2\text{Br}(\tilde{A}^2A'') + \text{Cl}(^2P)$ when \mathbf{D}^{Dyn} is intermediate between \mathbf{D} and the unit matrix is much more limited than at longer C-Cl distances.

The matrix multiplication of \mathbf{C}^{Dyn} and \mathbf{D}^{Dyn} generates the global transformation matrix, \mathbf{T}^{Dyn} , of eq 32. The scaling function for the elements of $\mathbf{H}^{\text{SO,F}}$ in the representation generated by \mathbf{T}^{Dyn} is the particularization of eq 34 to the BrCH_2Cl system and can be written as

$$\beta(m, \Delta) = \frac{\beta_{\text{Br}} (R_{\text{C-Br}} - R_{e,\text{C-Br}} + \Delta)^m + \beta_{\text{Cl}} (R_{\text{C-Cl}} - R_{e,\text{C-Cl}} + \Delta)^m}{(R_{\text{C-Br}} - R_{e,\text{C-Br}} + \Delta)^m + (R_{\text{C-Cl}} - R_{e,\text{C-Cl}} + \Delta)^m}, \quad (40)$$

where β_{Br} and β_{Cl} are equal to $-\frac{\Delta E_{\text{SO,Br}}}{3}$ and $-\frac{\Delta E_{\text{SO,Cl}}}{3}$, respectively, for the states that correlate with $\text{Br}(^2P_{3/2})$ and $\text{Cl}(^2P_{3/2})$, and β_{Br} equals $\frac{2\Delta E_{\text{SO,Br}}}{3}$ and β_{Cl} equals $\frac{2\Delta E_{\text{SO,Cl}}}{3}$ for the states that correlate with $\text{Br}(^2P_{1/2})$ and $\text{Cl}(^2P_{1/2})$. The symbols $R_{e,\text{C-Br}}$ and $R_{e,\text{C-Cl}}$ represent the respective equilibrium internuclear distances in the ground state of the BrCH_2Cl molecule. The parameters m and Δ were defined after eq 34. After some trial and error, the values $m = 4$ and $\Delta = 0.6 \text{ \AA}$ were chosen.

The F-diabatic potential matrix contains 24 energies along the diagonal and $24 \times 23/2 = 276$ F-diabatic couplings. The F-diabatic potential energy curves are shown in Figure 10. Continuous diabatic curves are obtained, and the states are distributed correctly into sets of eight (lowest fine-structure level) and four (highest fine-structure level) degenerate states in the dissociation limits. To test the accuracy of the F-diabatic representation, the F-adiabatic potential curves have been computed by diagonalization of the F-diabatic matrix and are presented in Figure 11. These potential curves should be compared with the *ab initio* F-adiabatic SA-CASSCF(12,8) curves shown in Figure 6. The MUEs of the approximate F-adiabatic energies have been computed including internuclear distances less or equal than 5.0 Å. Note that this is consistent with the way the MUEs were calculated for the HBr diatomic (see above), because here all C-Br and C-Cl internuclear distances are equal to or larger than the respective equilibrium distances. The MUEs of the approximate F-adiabatic energies oscillate between 0.04 eV for the ground state and 0.54 eV for one of the curves correlating with excited-state molecular fragments. The potential curves for the states that correlate with the ground states of fragments have MUEs in the range of 0.10–0.25 eV, comparable but somewhat larger than those found above for HBr. In contrast, the curves that correlate with the excited states of fragments have larger MUEs in the range of 0.10–0.54 eV. The largest errors are for the potential curves correlating with $\text{Br}(^2\text{P}_{3/2}) + \text{CH}_2\text{Cl}(\tilde{A} \ ^2A'')$ because the model triplet diabatic states that generate those curves are the least accurate, as can be seen in Figure 8 (t_4 and t_5). These results can be considered acceptable. In practice, the vertical excitation energies and dissociation energies can be improved by means of high-level theoretical or experimental data before fitting the resulting potential energy surfaces (for a range of geometries in configuration space) to multidimensional analytical functions.

4. Conclusions

We have devised an extension of the fourfold way diabatization scheme, developed previously for valence interactions, to construct diabatic representations suitable for spin-coupled systems. In this article we have formulated the method for the case of even-electron systems that yield pairs of fragments with doublet spin multiplicity. We have computed the valence diabatic representation of the singlet states by the fourfold way, and we have adopted valence-bond formulas to express the triplet diabatic energies in terms of singlet diabatic energies for polyatomic systems where bonds between doublet subsystems are broken; however, the method is more general, and it can be extended to doublet and quartet states and used with other methods of generating the valence diabatic states.

Generation of the triplet states from the singlets facilitates the computation of triplet diabatic potential energy surfaces because one is not required to identify dominant configuration lists for the triplet states. We have shown in an example that the approximation that the triplet diabatic couplings for the open-shell triplets are equal to the open-shell singlet ones is a very good approximation.

Two essential features of the method are (i) the introduction of a global transformation matrix as a product of channel-specific transformation matrices that depend on ratios of the spin-orbit constant and the valence splittings and (ii) the definition of spin-orbit coupling matrix elements as atomic matrix elements times a scaling function that depends on the internuclear distances. These improvements to the single-channel method allow one to study multichannel reactions with only as many diabatic states as the adiabatic states correlating with the electronic states of separate fragments relevant to the reaction dynamics. The new method affords a diabatic potential matrix with spin-orbit coupling that facilitates the calculation of

reaction probabilities and other properties in semiclassical dynamics simulations. Diabatic potential energy matrices including spin-orbit coupling have been constructed along bond-fission potential energy curves relevant to the photodissociation of two sample systems, HBr and BrCH₂Cl. A comparison between the spin-coupled adiabatic energies obtained with the new method and the *ab initio* adiabatic energies for these systems obtained with geometry-dependent spin-orbit coupling matrix elements shows that the method is sufficiently accurate for practical purposes. The method formulated here should be most useful for systems with a large number of atoms, especially heavy atoms, and/or a large number of spin-coupled electronic states.

Acknowledgment. This work was supported in part by the National Science Foundation under Grant Nos. CHE-0349122 and CHE0704974.

References

- 1 McGlynn, S. P.; Azumi, T.; Kinoshita, M. *Molecular Spectroscopy of the Triplet State*; Prentice-Hall: Englewood Cliffs, NJ, 1969.
- 2 Richards, W. G.; Trivedi, H. P.; Cooper, D. L. *Spin-Orbit Coupling in Molecules*; International Series of Monographs on Chemistry; Clarendon Press: Oxford, U.K., 1981.
- 3 Lefebvre-Brion, H.; Field, R. W. *Perturbations in the Spectra of Diatomic Molecules*; Academic Press: New York, 1986.
- 4 Hess, B. A.; Marian, C. M.; Peyerimhoff, S. D. In *Modern Electronic Structure Theory, Part I*; Yarkony, D. R., Ed.; World Scientific: Singapore, 1995; p. 152.
- 5 Ågren, H.; Vahtas, O.; Minaev, B. *Adv. Quantum Chem.* **1996**, 27, 71.
- 6 Marian, C. M. In *Reviews in Computational Chemistry*, Vol. 17; Lipowitz, K. B., Boyd, D. B., Eds.; Wiley-VCH: New York, 2001; Vol. 17, pp 99-204.
- 7 Fedorov, D. G.; Koseki, S.; Schmidt, M. W.; Gordon, M. S. *Int. Rev. Phys. Chem.* **2003**, 22, 551.
- 8 Havlas, Z.; Kyvala, M.; Michl, J. In *Molecular and Supramolecular Chemistry*; Kutateladze, A. G., Ed.; Computational Methods in Photochemistry, Vol. 13; CRC Press: Boca Raton, FL, 2005; pp 111-166.
- 9 Condon, E. U.; Shortley, G. H. *The Theory of Atomic Spectra*; Cambridge University Press: Cambridge, U.K., 1935.
- 10 Hougen, J. T.; *The Calculation of Rotational Energy Levels and Rotational Line Intensities in Diatomic Molecules*; National Bureau of Standards Monograph 115; National Bureau of Standards: Washington, DC, 1970.

- 11 Zare, R. N.; Schmeltekopf, A. L.; Harrop, W. J.; Albritton, D. L. *J. Mol. Spectrosc.* **1973**, *46*, 37.
- 12 Alexander, M. J.; Werner, H.-J.; Manolopoulos, D. E. *J. Chem. Phys.* **1998**, *109*, 5710.
- 13 Stark, K.; Werner, H.-J. *J. Chem. Phys.* **1996**, *104*, 6515.
- 14 Alexander, M. H.; Manolopoulos, D. E.; Werner, H.-J. *J. Chem. Phys.* **2000**, *113*, 11084.
- 15 Aquilanti, V.; Cavalli, S.; De Fazio, D.; Volpi, A.; Aguilar, A.; Giménez, X.; Lucas, J. M. *Phys. Chem. Chem. Phys.* **2002**, *4*, 401.
- 16 Corchado, J. C.; Truhlar, D. G.; Espinosa-Garcia, J. *J. Chem. Phys.* **2000**, *112*, 9375.
- 17 (a) Truhlar, D. G. *J. Chem. Phys.* **1972**, *56*, 3189; (b) Truhlar, D. G. *J. Chem. Phys.* **1974**, *61*, 440 (E).
- 18 Aquilanti, V.; Cavalli, S.; De Fazio, D.; Volpi, A.; Aguilar, A.; Giménez, X.; Lucas, J. M. *J. Chem. Phys.* **1985**, *109*, 3805.
- 19 Aquilanti, V.; Cavalli, S.; Pirani, F.; Volpi, A.; Cappelletti, D. *J. Phys. Chem. A* **2001**, *105*, 2401.
- 20 Aquilanti, V.; Cavalli, S.; De Fazio, D.; Volpi, A. *Int. J. Quantum Chem.* **2001**, *85*, 368.
- 21 Grinev, T. A.; Tscherbul, T. V.; Buchachenko, A. A.; Cavalli, S.; Aquilanti, V. *J. Phys. Chem. A* **2006**, *110*, 5458.
- 22 Skouteris, D.; Manolopoulos, D. E.; Bian, W.; Werner, H.-J.; Lai, L.-H.; Liu, K. *Science* **1999**, *286*, 1713.
- 23 Capecchi, G.; Werner, H.-J. *Phys. Chem. Chem. Phys.* **2004**, *6*, 4975.
- 24 Dubernet, M.-L.; Hutson, J. M. *J. Phys. Chem.* **1994**, *98*, 5844.
- 25 Schatz, G. C. *J. Phys. Chem.* **1995**, *99*, 7522.
- 26 Hankel, M.; Connor, J. N. L.; Schatz, G. C. *Chem. Phys.* **2005**, *225*, 308.

- 27 McClure, D. S. *J. Chem. Phys.* **1949**, *17*, 665.
- 28 Mizushima, M.; Koide, S. *J. Chem. Phys.* **1952**, *20*, 765.
- 29 Goodman, L.; Krishna, V. G. *J. Chem. Phys.* **1962**, *37*, 2721.
- 30 Salem, L.; Rowland, C. *Angew. Chem., Int. Ed.* **1972**, *11*, 92.
- 31 Koziar, J. C.; Cowan, D. O. *Acc. Chem. Res.* **1978**, *11*, 334.
- 32 Turro, N. J. *Modern Molecular Photochemistry*; University Science Books: Sausalito, CA, 1991.
- 33 Yarkony, D. R. *Int. Rev. Phys. Chem.* **1992**, *11*, 195.
- 34 Klessinger, M.; Michl, J. *Excited States and Photochemistry of Organic Molecules*; Wiley-VCH: New York, 1995.
- 35 Herzberg, G. *Molecular Spectra and Molecular Structure*, 2nd ed.; Van Nostrand: New York, 1950; Vol. 1, p 219.
- 36 Aquilanti, V.; Cavalli, S.; Volpi, A. *Phys. Essays* **2000**, *13*, 412.
- 37 Hoffmann, M. R.; Schatz, G. C. *J. Chem. Phys.* **2000**, *113*, 9456.
- 38 Maiti, B.; Schatz, G. C. *J. Chem. Phys.* **2003**, *119*, 12360.
- 39 Alexander, M. H.; Pouilly, B.; Duhoo, T. *J. Chem. Phys.* **1993**, *99*, 1752.
- 40 Mulliken, R. S. *Phys. Rev.* **1937**, *51*, 310.
- 41 Werner, H-J.; Rosmus, P. *J. Chem. Phys.* **1980**, *73*, 2319.
- 42 Chapman, D. A.; Balasubramanian, K.; Lin, S. H. *Chem. Phys.* **1987**, *118*, 333.
- 43 Seth, M.; Fischer, T.; Schwerdtfeger, P. *J. Chem. Soc., Faraday Trans.* **1996**, *92*, 167.
- 44 Pouilly, B.; Monnerville, M. *Chem. Phys.* **1998**, *238*, 437.
- 45 Smolin, A. G.; Vasyutinski, O. S.; Balint-Kurti, G. G.; Brown, A. J. *Phys. Chem. A* **2006**, *110*, 5371.

- 46 Yabushita, S.; Morokuma, K. *Chem. Phys. Lett.* **1990**, *175*, 518.
- 47 Amamatsu, Y.; Morokuma, K.; Yabushita, S. *J. Chem. Phys.* **1991**, *94*, 4858.
- 48 Amamatsu, Y.; Yabushita, S.; Morokuma, K. *J. Chem. Phys.* **1996**, *104*, 9783.
- 49 Xie, D. Q.; Guo, H.; Amamatsu, Y.; Kosloff, R. *J. Phys. Chem. A* **2000**, *104*, 1009.
- 50 Ajitha, D.; Wierzbowska, M.; Lindh, R.; Malmqvist, P. A. *J. Chem. Phys.* **2004**, *121*, 5761.
- 51 Yabushita, S.; Morokuma, K. *Chem. Phys. Lett.* **1990**, *175*, 518.
- 52 Amamatsu, Y.; Yabushita, S.; Morokuma, K. *J. Chem. Phys.* **1994**, *100*, 4894.
- 53 Coronado, E. A.; Batista, V. S.; Miller, W. H. *J. Chem. Phys.* **2000**, *112*, 5566.
- 54 Batista, V. S.; Brumer, P. *J. Phys. Chem. A* **2001**, *105*, 2591.
- 55 Rozgonyi, T.; Feurer, T.; González, L. *Chem. Phys. Lett.* **2001**, *350*, 155.
- 56 Rozgonyi, T.; González, L. *J. Phys. Chem. A* **2002**, *106*, 11150.
- 57 Zhou, J.; Lau, K.-C.; Hassanein, E.; Xu, H.; Tian, S.-X.; Jones, B.; Ng, C. Y. *J. Chem. Phys.* **2006**, *124*, 034309.
- 58 Rozgonyi, T.; González, L. *J. Phys. Chem. A* **2006**, *110*, 10251.
- 59 Marks, A. J. *J. Chem. Phys.* **2001**, *114*, 1700.
- 60 Ding, W.-J.; Fang, W.-H.; Liu, R.-Z.; Fang, D.-C. *J. Chem. Phys.* **2002**, *117*, 8745.
- 61 Bacchus-Montabonel, M.-C.; Vaeck, N.; Lasorne, B.; Desouter-Lecomte, M. *Chem. Phys. Lett.* **2003**, *374*, 307.
- 62 Lasorne, B.; Bacchus-Montabonel, M.-C.; Vaeck, N.; Desouter-Lecomte, M. *J. Chem. Phys.* **2004**, *120*, 1271.
- 63 Zhang, F.; Ding, W.-J.; Fang, W.-H. *J. Chem. Phys.* **2006**, *125*, 184305.
- 64 Valero, R.; Truhlar, D. G. *J. Chem. Phys.* **2006**, *125*, 194305.

- 65 Mulliken, R. S. *Phys. Rev.* **1929**, 33, 730.
- 66 Mulliken, R. S. *Rev. Mod. Phys.* **1932**, 4, 1.
- 67 McClure, D. S. *J. Chem. Phys.* **1949**, 17, 905.
- 68 Stone, A. J. *Proc. R. Soc. London, Ser. A* **1963**, 271, 424.
- 69 Ishiguro, E.; Kobori, M. *J. Phys. Soc. Jpn.* **1967**, 22, 263.
- 70 Moores, W. H.; McWeeny, R. *Proc. Royal Soc. London, Ser. A* **1973**, 332, 365.
- 71 Langhoff, S. R. *J. Chem. Phys.* **1980**, 73, 2379.
- 72 Hay, P. J.; Wadt, W. R.; Kahn, L. R.; Raffanetti, R. C.; Phillips, D. H. *J. Chem. Phys.* **1979**, 71, 1767.
- 73 Cohen, J. S.; Wadt, W. R.; Hay, P. J. *J. Chem. Phys.* **1979**, 71, 2955.
- 74 Hay, P. J. *J. Am. Chem. Soc.* **1982**, 104, 7007.
- 75 Hay, P. J. *J. Chem. Phys.* **1983**, 79, 5469.
- 76 Heinemann, C.; Koch, W.; Schwarz, H. *Chem. Phys. Lett.* **1995**, 245, 509.
- 77 Kinnersly, S. R.; Murrell, J. N.; Rodwell, W. R. *J. Chem. Soc. Faraday Trans. 2* **1978**, 74, 600.
- 78 Angeli, C.; Persico, M. *Chem. Phys.* **1996**, 204, 57. See also: Kokoouline, V.; Dulieu, O.; Masnou-Seeuws, F. *Phys. Rev. A* **2000**, 62, 22504.
- 79 Tully, J. C. *J. Chem. Phys.* **1973**, 59, 5122.
- 80 Cohen, J. S.; Schneider, B. *J. Chem. Phys.* **1974**, 61, 3230.
- 81 Hay, P. J.; Dunning, T. H.; Raffanetti, R. C. *J. Chem. Phys.* **1976**, 65, 2679.
- 82 Hay, P. J.; Dunning, T. H. *J. Chem. Phys.* **1977**, 66, 1306.
- 83 Stevens, W. J.; Gardner, M.; Karo, A.; Julienne, P. *J. Chem. Phys.* **1977**, 67, 2860.
- 84 Wadt, W. R. *J. Chem. Phys.* **1978**, 68, 402.

- 85 Huestis, D. L.; Schlotter, N. E. *J. Chem. Phys.* **1978**, *69*, 3100.
- 86 Grein, F.; Peyerimhoff, S. D. *J. Chem. Phys.* **1987**, *87*, 4684.
- 87 Amarouche, M.; Durand, G.; Malrieu, J. P. *J. Chem. Phys.* **1988**, *88*, 1010.
- 88 Naumkin, F. Y. *Chem. Phys.* **1998**, *226*, 319.
- 89 Vieuxmaire, O. P. J.; Nix, M. G. D.; Fitzpatrick, J. A. J.; Beckert, M.; Dixon, R. N.; Ashfold, M. N. R. *Phys. Chem. Chem. Phys.* **2004**, *6*, 543.
- 90 Bonhommeau, D.; Halberstadt, N.; Viel, A. *J. Chem. Phys.* **2006**, *124*, 184314.
- 91 Mielke, S. L.; Truhlar, D. G.; Schwenke, D. W. *J. Phys. Chem.* **1995**, *99*, 16210.
- 92 Nakamura, H.; Truhlar, D. G. *J. Chem. Phys.* **2001**, *115*, 10353.
- 93 Nakamura, H.; Truhlar, D. G. *J. Chem. Phys.* **2002**, *117*, 5576.
- 94 Nakamura, H.; Truhlar, D. G. *J. Chem. Phys.* **2003**, *118*, 6816.
- 95 Van Vleck, J. H. *Phys. Rev.* **1934**, *45*, 405.
- 96 Serber, R. *Phys. Rev.* **1934**, *45*, 461.
- 97 Stehn, J. R. *J. Chem. Phys.* **1937**, *5*, 186.
- 98 Blais, N. C.; Truhlar, D. G. *J. Chem. Phys.* **1973**, *58*, 1090.
- 99 Sato, S. *Bull. Chem. Soc. Japan* **1955**, *28*, 450.
- 100 Kuntz, P. J.; Nemeth, E. M.; Polanyi, J. C.; Rosner, S. D.; Young, C. E. *J. Chem. Phys.* **1966**, *44*, 1168.
- 101 Eyring, H.; Polanyi, M. *Naturwissenschaften* **1930**, *18*, 914.
- 102 Glasstone, S.; Laidler, K. J.; Eyring, H. *The Theory of Rate Processes*; McGraw-Hill: New York, 1941.
- 103 Truhlar, D. G.; Wyatt, R. E. *Adv. Chem. Phys.* **1977**, *36*, 141.
- 104 Mies, F. H. *Phys. Rev. A* **1973**, *7*, 942.

- 105 Aquilanti, V.; Grossi, G. *J. Chem. Phys.* **1980**, *73*, 1165.
- 106 Aquilanti, V.; Casavecchia, P.; Grossi, G.; Laganá, A. *J. Chem. Phys.* **1980**, *73*, 1173.
- 107 Dubernet, M.-L.; Hutson, J. M. *J. Phys. Chem.* **1994**, *98*, 5844.
- 108 Fishchuk, A. V.; Groenenboom, G. C.; van der Avoird, A. *J. Phys. Chem. A* **2006**, *110*, 5280.
- 109 Cohen, J. S.; Collins, L. A.; Lane, N. F. *Phys. Rev. A* **1978**, *17*, 1343.
- 110 Werner, H.-J.; Knowles, P. J.; Lindh, R.; Manby, F. R.; Schütz, M.; Celani, P.; Korona, T.; Manby, F. R.; Rauhut, G.; Amos, R. D.; Bernhardsson, A.; Berning, A.; Cooper, D. L.; Deegan, M. J. O.; Dobbyn, A. J.; Eckert, F.; Hampel, C.; Hetzer, G.; Lloyd, A. W.; McNicholas, S. J.; Meyer, W.; Mura, M. E.; Nicklass, A.; Palmieri, P.; Pitzer, R.; Schumman, U.; Stoll, H.; Stone, A. J.; Tarroni, R.; Thorsteinsson, T. *MOLPRO: A Package of Ab Initio Programs*, version 2002.6; 2004. <http://www.molpro.net>.
- 111 Werner, H.-J.; Knowles, P. J. *J. Chem. Phys.* **1985**, *82*, 5053.
- 112 Knowles, P. J.; Werner, H.-J. *Chem. Phys. Lett.* **1985**, *115*, 259.
- 113 Berning, A.; Schweizwer, M.; Werner, H.-J.; Knowles, P. J.; Palmieri, P. *Mol. Phys.* **2000**, *98*, 1823.
- 114 Krishnan, R.; Binkley, J. S.; Seeger, R.; Pople, J. A. *J. Chem. Phys.* **1980**, *72*, 650.
- 115 (a) Dunning, T. H., Jr. *J. Chem. Phys.* **1977**, *66*, 1382. (b) Binning, R. C.; Curtiss, L. A. *J. Comput. Chem.* **1990**, *11*, 1206.
- 116 Moore, C. E. *Atomic Energy Levels*; Circular 467; National Bureau of Standards: Washington, DC, 1949; Vol. 1-3.
- 117 Nicklass, A.; Peterson, K. A.; Berning, A.; Werner, H.-J.; Knowles, P. J. *J. Chem. Phys.* **2000**, *112*, 5624.

- 118 Schmidt, M. W.; Baldrige, K. K.; Boatz, J. A.; Elbert, S. T.; Gordon, M. S.; Jensen, J. H.; Koseki, S.; Matsunaga, N.; Nguyen, K. A.; Su, S. J.; Windus, T. L.; Dupuis, M.; Montgomery, J. A. *J. Comput. Chem.* **1993**, *14*, 1347.
- 119 (a) Hariharan, P. C.; Pople, J. A. *Theor. Chim. Acta* **1973**, *28*, 213. (b) Francl, M. M.; Pietro, W. J.; Hehre, W. J.; Binkley, J. S.; Gordon, M. S.; DeFrees, D. J.; Pople, J. A. *J. Chem. Phys.* **1982**, *77*, 3654. (c) Rassolov, V.; Pople, J. A.; Ratner, M.; Windus, T. L. *J. Chem. Phys.* **1998**, *109*, 1223.
- 120 Frisch, M. J.; Trucks, G. W.; Schlegel, H. B.; Scuseria, G. E.; Robb, M. A.; Cheeseman, J. R.; Montgomery, J. A., Jr.; Vreven, T.; Kudin, K. N.; Burant, J. C.; Millam, J. M.; Iyengar, S. S.; Tomasi, J.; Barone, V.; Mennucci, B.; Cossi, M.; Scalmani, G.; Rega, N.; Petersson, G. A.; Nakatsuji, H.; Hada, M.; Ehara, M.; Toyota, K.; Fukuda, R.; Hasegawa, J.; Ishida, M.; Nakajima, T.; Honda, Y.; Kitao, O.; Nakai, H.; Klene, M.; Li, X.; Knox, J. E.; Hratchian, H. P.; Cross, J. B.; Bakken, V.; Adamo, C.; Jaramillo, J.; Gomperts, R.; Stratmann, R. E.; Yazyev, O.; Austin, A. J.; Cammi, R.; Pomelli, C.; Ochterski, J. W.; Ayala, P. Y.; Morokuma, K.; Voth, G. A.; Salvador, P.; Dannenberg, J. J.; Zakrzewski, V. G.; Dapprich, S.; Daniels, A. D.; Strain, M. C.; Farkas, O.; Malick, D. K.; Rabuck, A. D.; Raghavachari, K.; Foresman, J. B.; Ortiz, J. V.; Cui, Q.; Baboul, A. G.; Clifford, S.; Cioslowski, J.; Stefanov, B. B.; Liu, G.; Liashenko, A.; Piskorz, P.; Komaromi, I.; Martin, R. L.; Fox, D. J.; Keith, T.; Al-Laham, M. A.; Peng, C. Y.; Nanayakkara, A.; Challacombe, M.; Gill, P. M. W.; Johnson, B.; Chen, W.; Wong, M. W.; Gonzalez, C.; Pople, J. A. *Gaussian 03*, revision D.01 ; Gaussian, Inc.: Wallingford, CT, 2004.
- 121 (a) Nakamura, H.; Xidos, J. D.; Chamberlin, A. C.; Kelly, K. C.; Valero, R.; Thompson, J. D.; Li, J.; Hawkins, G. D.; Zhu, T.; Lynch, B. J.; Volobuev, Y.; Rinaldi, D.; Liotard,

- D. A.; Cramer, C. J.; Truhlar, D. G. *HONDOPLUS*, version 5.1, based on *HONDO*, version 99.6; University of Minnesota: Minneapolis, MN, 2007. (b) Dupuis, M.; Marquez, A.; Davidson, E. R. *HONDO*, version 99.6, based on *HONDO*, version 95.3, Quantum Chemistry Program Exchange, Indiana University: Bloomington, IN, 1999.
- 122 Jasper, A. W.; Kendrick, B. K.; Mead, C. A.; Truhlar, D. G. *Adv. Ser. Phys. Chem.* **2004**, *14*, 329.

TABLE 1: Comparison of Representations

<u>Nonzero off-diagonal elements</u>						
Representation	also called	Abbrev.	H^{Val}	H^{SO}	H^{Elec}	Nonadiabatic coupling ^a
Valence adiabatic	spin-free adiabatic	V-a	no	yes	–	not negligible
Valence diabatic	spin-free diabatic	V-d	yes	yes	–	assumed negligible
Fully adiabatic	spin-valence adiabatic	F-a	–	–	no	not negligible
Fully diabatic	spin-valence diabatic	F-d	–	–	yes	assumed negligible

^a “Nonadiabatic coupling” is due to the operation of the nuclear kinetic energy or nuclear momentum operator on the electronic wave function, with the vector coupling due to nuclear momentum dominating in the semiclassical limit. In contrast, diabatic states are assumed to be coupled by a scalar operator associated with nondiagonal matrix elements of the electronic Hamiltonian; this is called “diabatic coupling”. See ref 122.

TABLE 2: Elements of the Matrix of H^{SO} in the v-Diabatic Representation^a

				$^1\Sigma$	$^3\Pi_x$	$^3\Pi_y$	$^1\Pi_x$	$^3\Sigma$	$^3\Pi_y$	$^1\Pi_y$	$^3\Sigma$	$^3\Pi_x$	$^3\Sigma$	$^3\Pi_x$	$^3\Pi_y$
$^1\Sigma$	s_0	s_5	0	0.0	$-\lambda$	$-\lambda i$	0.0	0.0	0.0	0.0	0.0	0.0	0.0	0.0	0.0
$^3\Pi_x$	t_3	t_5	1+	$-\lambda$	0.0	λi	0.0	0.0	0.0	0.0	0.0	0.0	0.0	0.0	0.0
$^3\Pi_y$	t_2	t_4	1-	λi	$-\lambda i$	0.0	0.0	0.0	0.0	0.0	0.0	0.0	0.0	0.0	0.0
$^1\Pi_x$	s_2	s_4	0	0.0	0.0	0.0	0.0	$-\lambda$	$-\lambda i$	0.0	0.0	0.0	0.0	0.0	0.0
$^3\Sigma$	t_1	t_6	1+	0.0	0.0	0.0	$-\lambda$	0.0	λi	0.0	0.0	0.0	0.0	0.0	0.0
$^3\Pi_y$	t_2	t_4	0	0.0	0.0	0.0	λi	$-\lambda i$	0.0	0.0	0.0	0.0	0.0	0.0	0.0
$^1\Pi_y$	s_1	s_3	0	0.0	0.0	0.0	0.0	0.0	0.0	0.0	$-\lambda i$	λi	0.0	0.0	0.0
$^3\Sigma$	t_1	t_6	1-	0.0	0.0	0.0	0.0	0.0	0.0	λi	0.0	$-\lambda$	0.0	0.0	0.0
$^3\Pi_x$	t_3	t_5	0	0.0	0.0	0.0	0.0	0.0	0.0	$-\lambda i$	$-\lambda$	0.0	0.0	0.0	0.0
$^3\Sigma$	t_1	t_6	0	0.0	0.0	0.0	0.0	0.0	0.0	0.0	0.0	0.0	0.0	λ	λi
$^3\Pi_x$	t_3	t_5	1-	0.0	0.0	0.0	0.0	0.0	0.0	0.0	0.0	0.0	λ	0.0	λi
$^3\Pi_y$	t_2	t_4	1+	0.0	0.0	0.0	0.0	0.0	0.0	0.0	0.0	0.0	$-\lambda i$	$-\lambda i$	0.0

^a For HBr, this is equal to the full $\mathbf{H}^{SO,Val}$ matrix. For BrCH₂Cl, this matrix is a subblock of the full $\mathbf{H}^{SO,Val}$ matrix (see eq 19). The symbols in the first four columns indicate the v-diabatic states. The first symbols refer to the spatial symmetry of the v-diabatic states of HBr; the second and third symbols refer to Br(²P) + CH₂Cl(\tilde{X}^2A') and to Br(²P) + CH₂Cl(\tilde{A}^2A'), respectively; and the last symbols refer to the spin symmetry (see text). The same symbols as in these columns should be above columns 2-13; for brevity, only the spatial symmetry of the v-diabatic states of HBr is indicated. For the nonzero elements of the matrix, λ is defined as $\Delta E_{SO} / 3$, where ΔE_{SO} is the spin-orbit fine-structure splitting of bromine or chlorine, and i denotes $\sqrt{-1}$.

TABLE 3: Elements of the $\mathbf{C}^{(n)}$ Transformation Matrix^a

				$j_{Br} = \frac{3}{2}$	$j_{Br} = \frac{3}{2}$	$j_{Br} = \frac{1}{2}$	$j_{Br} = \frac{3}{2}$	$j_{Br} = \frac{1}{2}$	$j_{Br} = \frac{3}{2}$	$j_{Br} = \frac{3}{2}$	$j_{Br} = \frac{1}{2}$	$j_{Br} = \frac{3}{2}$	$j_{Br} = \frac{1}{2}$	$j_{Br} = \frac{3}{2}$	$j_{Br} = \frac{3}{2}$
¹ Σ	s ₀	s ₅	0	.8165	0.0	-.5774	0.0	0.0	0.0	0.0	0.0	0.0	0.0	0.0	0.0
³ Π_x	t ₃	t ₅	1+	.4082	.7071	.5774	0.0	0.0	0.0	0.0	0.0	0.0	0.0	0.0	0.0
³ Π_y	t ₂	t ₄	1-	-.4082 i	.7071 i	-.5774 i	0.0	0.0	0.0	0.0	0.0	0.0	0.0	0.0	0.0
¹ Π_x	s ₂	s ₄	0	0.0	0.0	0.0	.6295	-.5774	-.5200	0.0	0.0	0.0	0.0	0.0	0.0
³ Σ	t ₁	t ₆	1+	0.0	0.0	0.0	.7651	.5774	.2852	0.0	0.0	0.0	0.0	0.0	0.0
³ Π_y	t ₂	t ₄	0	0.0	0.0	0.0	.1355 i	-.5774 i	.8052 i	0.0	0.0	0.0	0.0	0.0	0.0
¹ Π_y	s ₁	s ₃	0	0.0	0.0	0.0	0.0	0.0	0.0	.6295	.5774	.5200	0.0	0.0	0.0
³ Σ	t ₁	t ₆	1-	0.0	0.0	0.0	0.0	0.0	0.0	-.7651 i	.5774 i	.2852 i	0.0	0.0	0.0
³ Π_x	t ₃	t ₅	0	0.0	0.0	0.0	0.0	0.0	0.0	-.1355 i	-.5774 i	.8052 i	0.0	0.0	0.0
³ Σ	t ₁	t ₆	0	0.0	0.0	0.0	0.0	0.0	0.0	0.0	0.0	0.0	.5774	0.0	.8165
³ Π_x	t ₃	t ₅	1-	0.0	0.0	0.0	0.0	0.0	0.0	0.0	0.0	0.0	.5774	.7071	-.4082
³ Π_y	t ₂	t ₄	1+	0.0	0.0	0.0	0.0	0.0	0.0	0.0	0.0	0.0	-.5774 i	.7071 i	.4082 i

^a In this table, $n = 12$. For HBr, the $\mathbf{C}^{(n)}$ matrix is equal to the full \mathbf{C} matrix. For BrCH₂Cl, the $\mathbf{C}^{(n)}$ matrix is a subblock of the full \mathbf{C} matrix (see eq 20). The symbols in the first four columns indicate the v-diabatic states as in Table 2. The symbols above columns 2-13 indicate the value of the total electronic angular momentum of the bromine atom, j_{Br} , in the dissociation limit for each of the F-diabatic states.

TABLE 4: Diabatic Group Lists for the Four Singlet and Four Triplet v-diabatic States of BrCH₂Cl Obtained Using the Fourfold Way^a

Group 1	$\chi_1: p_{\sigma}(\text{Cl})^2 p_{\sigma}(\text{Br})^2 p_{\pi}(\text{Cl})^2 p'_{\pi}(\text{Cl})^2 p_{\pi}(\text{Br})^2 p'_{\pi}(\text{Br})^1 u^{*1} v^{*0}$
	$\chi_2: p_{\sigma}(\text{Cl})^2 p_{\sigma}(\text{Br})^2 p_{\pi}(\text{Cl})^2 p'_{\pi}(\text{Cl})^2 p_{\pi}(\text{Br})^2 p'_{\pi}(\text{Br})^1 u^{*0} v^{*1}$
	$\chi_3: p_{\sigma}(\text{Cl})^1 p_{\sigma}(\text{Br})^2 p_{\pi}(\text{Cl})^2 p'_{\pi}(\text{Cl})^2 p_{\pi}(\text{Br})^2 p'_{\pi}(\text{Br})^1 u^{*0} v^{*2}$
Group 2	$\chi_4: p_{\sigma}(\text{Cl})^2 p_{\sigma}(\text{Br})^2 p_{\pi}(\text{Cl})^2 p'_{\pi}(\text{Cl})^2 p_{\pi}(\text{Br})^1 p'_{\pi}(\text{Br})^2 u^{*1} v^{*0}$
	$\chi_5: p_{\sigma}(\text{Cl})^2 p_{\sigma}(\text{Br})^2 p_{\pi}(\text{Cl})^2 p'_{\pi}(\text{Cl})^2 p_{\pi}(\text{Br})^1 p'_{\pi}(\text{Br})^2 u^{*0} v^{*1}$
	$\chi_6: p_{\sigma}(\text{Cl})^2 p_{\sigma}(\text{Br})^2 p_{\pi}(\text{Cl})^2 p'_{\pi}(\text{Cl})^1 p_{\pi}(\text{Br})^2 p'_{\pi}(\text{Br})^1 u^{*0} v^{*2}$
Group 3	$\chi_7: p_{\sigma}(\text{Cl})^2 p_{\sigma}(\text{Br})^2 p_{\pi}(\text{Cl})^2 p'_{\pi}(\text{Cl})^1 p_{\pi}(\text{Br})^2 p'_{\pi}(\text{Br})^2 u^{*1} v^{*0}$
	$\chi_8: p_{\sigma}(\text{Cl})^2 p_{\sigma}(\text{Br})^2 p_{\pi}(\text{Cl})^2 p'_{\pi}(\text{Cl})^1 p_{\pi}(\text{Br})^2 p'_{\pi}(\text{Br})^2 u^{*0} v^{*1}$
	$\chi_9: p_{\sigma}(\text{Cl})^2 p_{\sigma}(\text{Br})^1 p_{\pi}(\text{Cl})^2 p'_{\pi}(\text{Cl})^1 p_{\pi}(\text{Br})^2 p'_{\pi}(\text{Br})^2 u^{*2} v^{*0}$
Group 4	$\chi_{10}: p_{\sigma}(\text{Cl})^2 p_{\sigma}(\text{Br})^2 p_{\pi}(\text{Cl})^1 p'_{\pi}(\text{Cl})^2 p_{\pi}(\text{Br})^2 p'_{\pi}(\text{Br})^2 u^{*1} v^{*0}$
	$\chi_{11}: p_{\sigma}(\text{Cl})^2 p_{\sigma}(\text{Br})^2 p_{\pi}(\text{Cl})^1 p'_{\pi}(\text{Cl})^2 p_{\pi}(\text{Br})^2 p'_{\pi}(\text{Br})^2 u^{*0} v^{*1}$
	$\chi_{12}: p_{\sigma}(\text{Cl})^2 p_{\sigma}(\text{Br})^2 p_{\pi}(\text{Cl})^2 p'_{\pi}(\text{Cl})^1 p_{\pi}(\text{Br})^2 p'_{\pi}(\text{Br})^1 u^{*2} v^{*0}$

^a p_{π} and p'_{π} represent nonbonding orbitals parallel and orthogonal to the molecular plane, respectively, and p_{σ} a bonding orbital of the halogen atoms for short values of the C-Br and C-Cl bond distances. “u*” is a DMO that corresponds mainly to $\sigma^*(\text{C-Br})$, and “w*” is mainly $\sigma^*(\text{C-Cl})$.

FIGURE CAPTIONS

FIG. 1. SA-CASSCF(6,4) v-diabatic potential energy curves for the HBr molecule derived from $H(^2S) + Br(^2P)$.

FIG. 2. SA-CASSCF(6,4) F-adiabatic potential energy curves for the HBr molecule correlating with the $H(^2S) + Br(^2P_{3/2})$ (lower) and $H(^2S) + Br(^2P_{1/2})$ (higher) fine-structure levels.

FIG. 3. Five unique SA-CASSCF(6,4) spin-orbit coupling matrix elements as a function of the H-Br distance. Note that the curves for the $\langle ^3\Pi_1 | H^{SO} | ^1\Pi_1 \rangle$ and $\langle ^3\Pi_0 | H^{SO} | ^3\Pi_0 \rangle$ matrix elements practically overlap over the whole H-Br distance range represented.

FIG. 4. Comparison of SA-CASSCF(6,4) v-diabatic triplet potential curves (solid lines) with those derived from the model in eqs 3–9 (dashed lines) for the HBr molecule. The constants of the model (eqs 5a and 5b) were determined at (a) $R = 1.45 \text{ \AA}$ and (b) $R = 2.0 \text{ \AA}$.

FIG. 5. F-adiabatic potential energy curves constructed from SA-CASSCF(6,4) singlet potential curves and model triplet potential curves for the HBr molecule. The v-diabatic triplet potential curves used are the model curves shown in Figure 4a.

FIG. 6. SA-CASSCF(12,8) F-adiabatic potential energy curves for the $BrCH_2Cl$ molecule. The abscissa values are referenced to the respective equilibrium distances of ground-state $BrCH_2Cl$, i.e., $\Delta R(C-Br) \equiv 1.934 \text{ \AA} - R(C-Br)$ and $\Delta R(C-Cl) \equiv R(C-Cl) - 1.763 \text{ \AA}$.

FIG. 7. v -diabatic singlet potential energy curves for the BrCH_2Cl molecule. The v -diabatic states s_1 , s_2 , s_3 , and s_4 were obtained by the fourfold way from SA-CASSCF(12,8) wave functions and energies, whereas s_0 and s_5 are taken as the lowest and the highest v -adiabatic states, respectively. The state numbering corresponds to the diabatic groups presented in Table 4. The C-Cl and C-Br bond distances are referenced to the respective equilibrium distances of ground-state BrCH_2Cl .

FIG. 8. v -diabatic triplet potential energy curves for the BrCH_2Cl molecule obtained from v -adiabatic SA-CASSCF(12,8) wave functions and energies (a) by the fourfold way and (b) using the new method (b). The v -diabatic states t_2 , t_3 , t_4 , and t_5 along the C-Br bond-scission coordinate and t_1 , t_2 , t_3 , t_4 , and t_5 along the C-Cl bond-scission coordinate were computed by the fourfold way, and the other states are taken as the v -adiabatic states. The state numbering corresponds to the diabatic groups presented in Table 4. The C-Cl and C-Br bond distances are referenced to the respective equilibrium distances of ground-state BrCH_2Cl .

FIG. 9. v -diabatic couplings for the BrCH_2Cl molecule obtained from v -adiabatic SA-CASSCF(12,8) wave function and energies by the fourfold way. The singlet couplings (solid lines) are compared with the triplet couplings (dashed lines). The state numbering corresponds to the diabatic groups presented in Table 4. The C-Cl and C-Br bond distances are referenced to the respective equilibrium distances of ground-state BrCH_2Cl .

FIG. 10. F-diabatic potential energy curves for the BrCH_2Cl molecule constructed with the new method. The C-Cl and C-Br bond distances are referenced to the respective equilibrium distances of ground-state BrCH_2Cl .

FIG. 11. F-adiabatic potential energy curves for the BrCH_2Cl molecule obtained from diagonalization of the F-diabatic potential matrix constructed with the new method. The C-Cl and C-Br bond distances are referenced to the respective equilibrium distances of ground-state BrCH_2Cl .

Figure 1

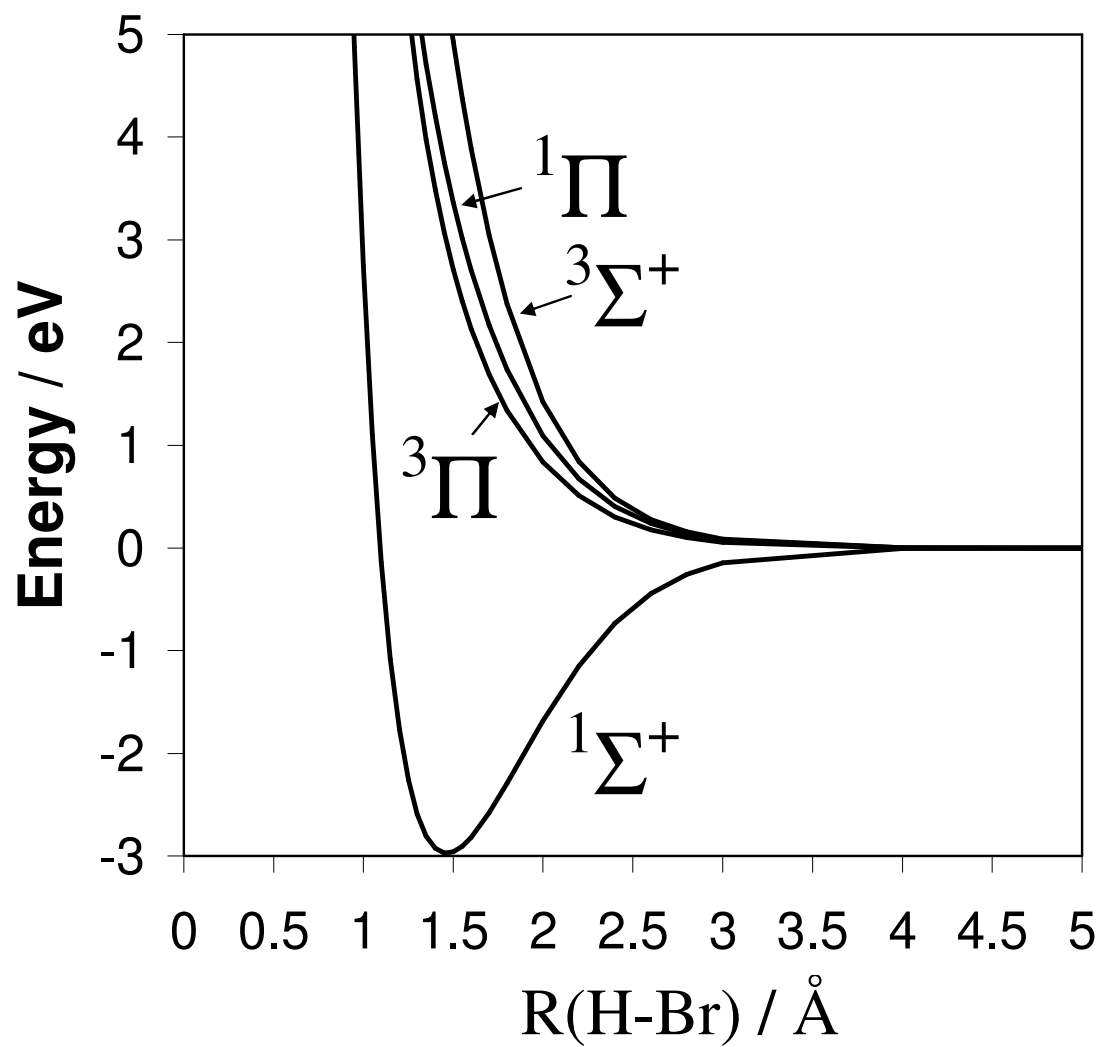


Figure 2

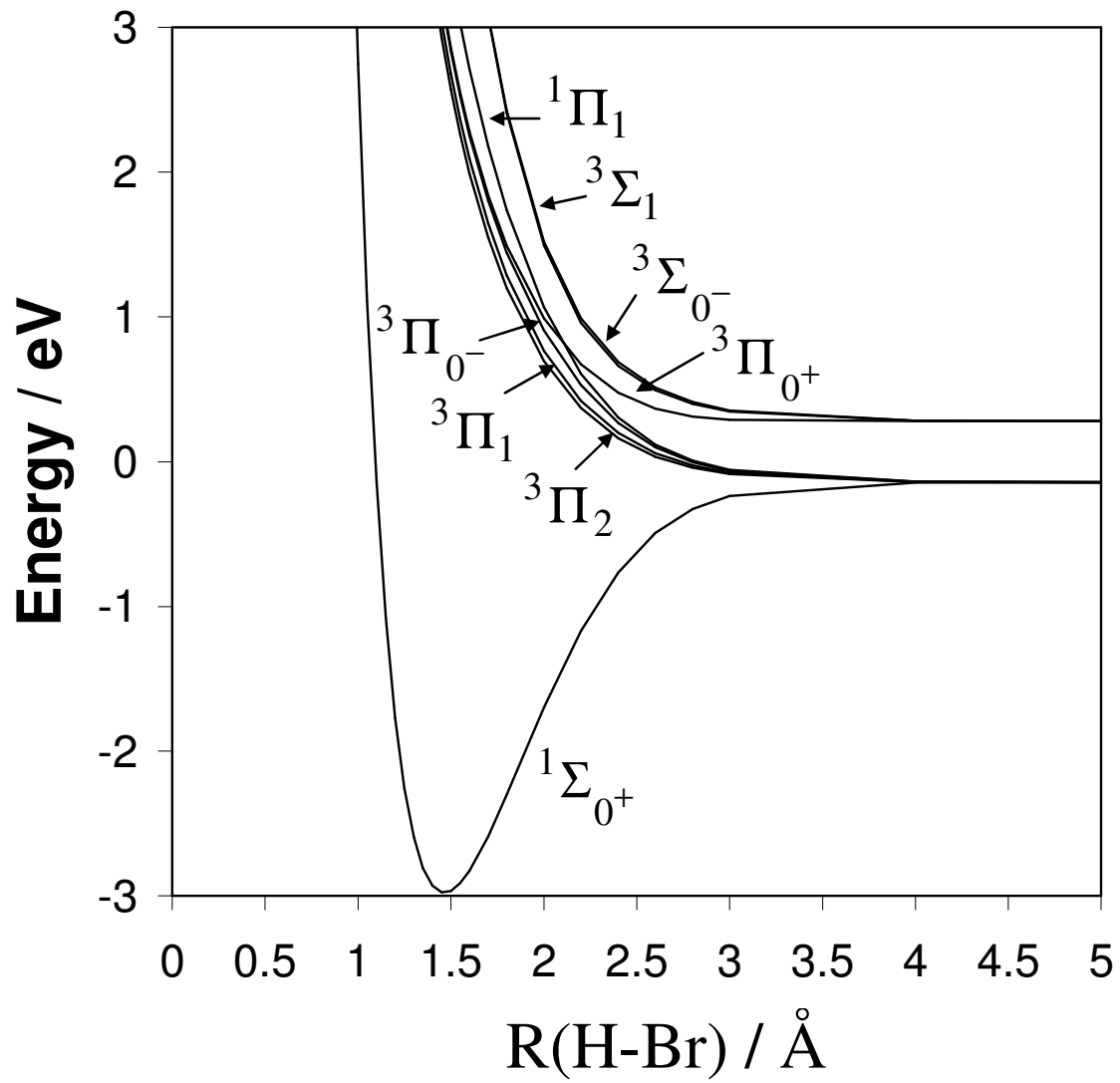


Figure 3

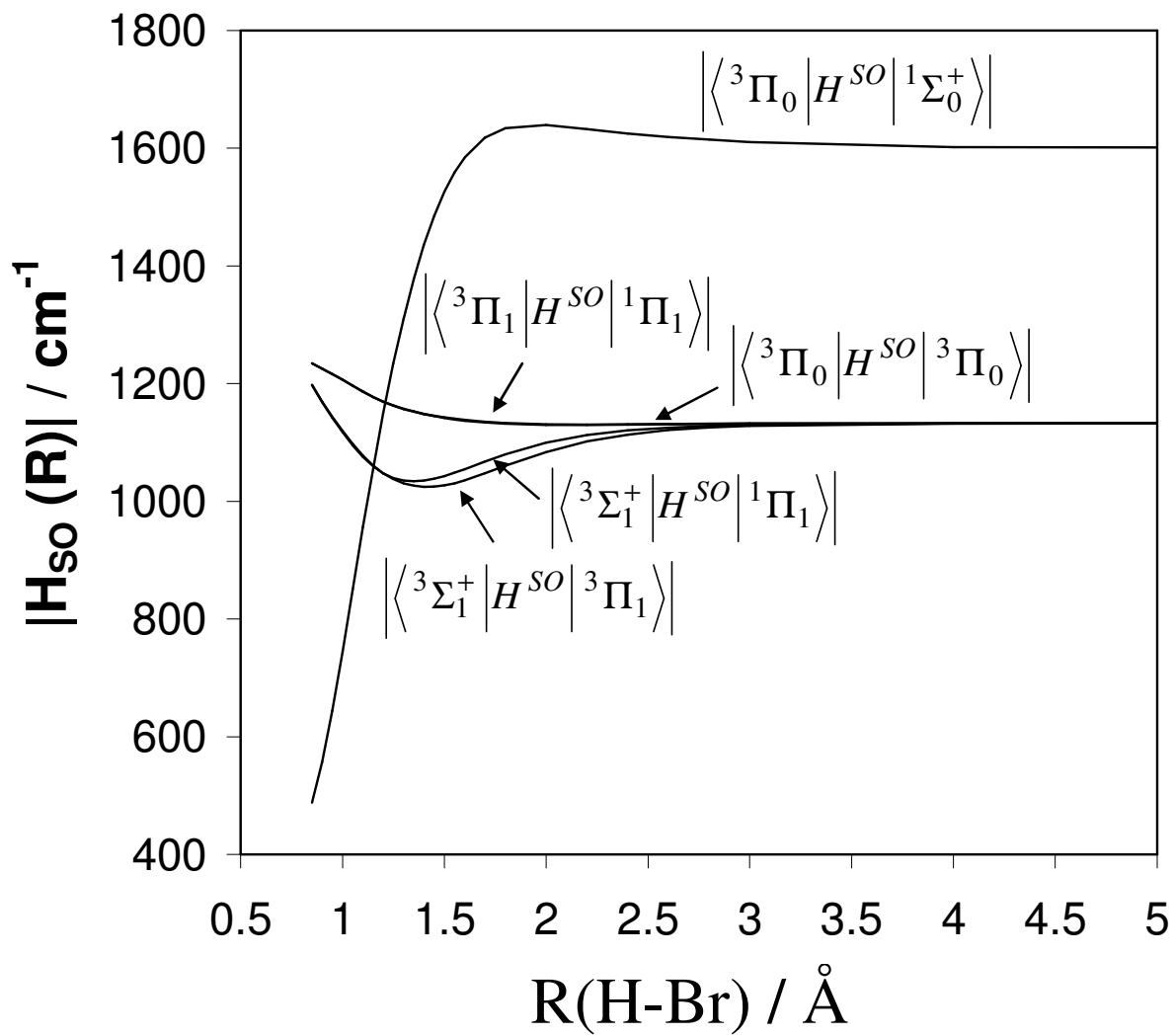


Figure 4

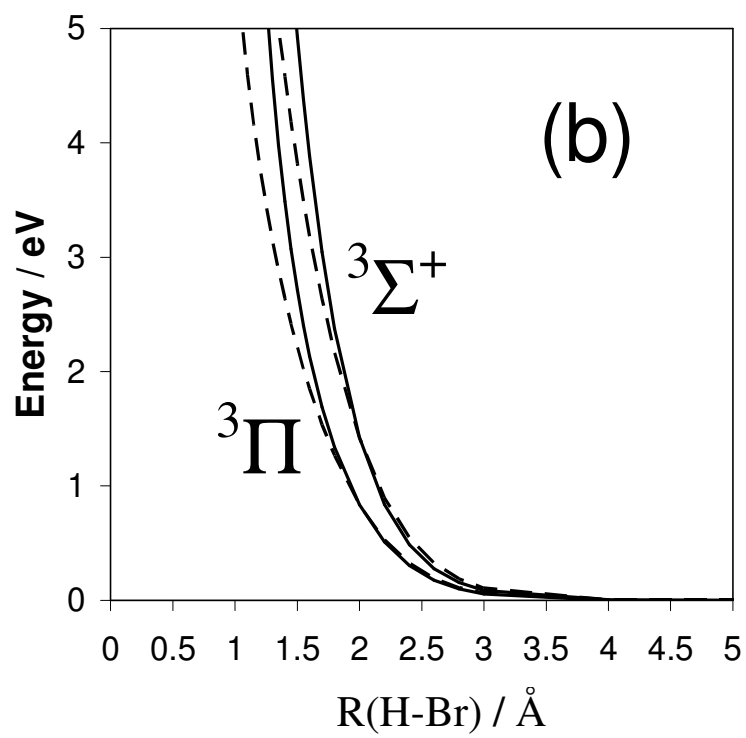
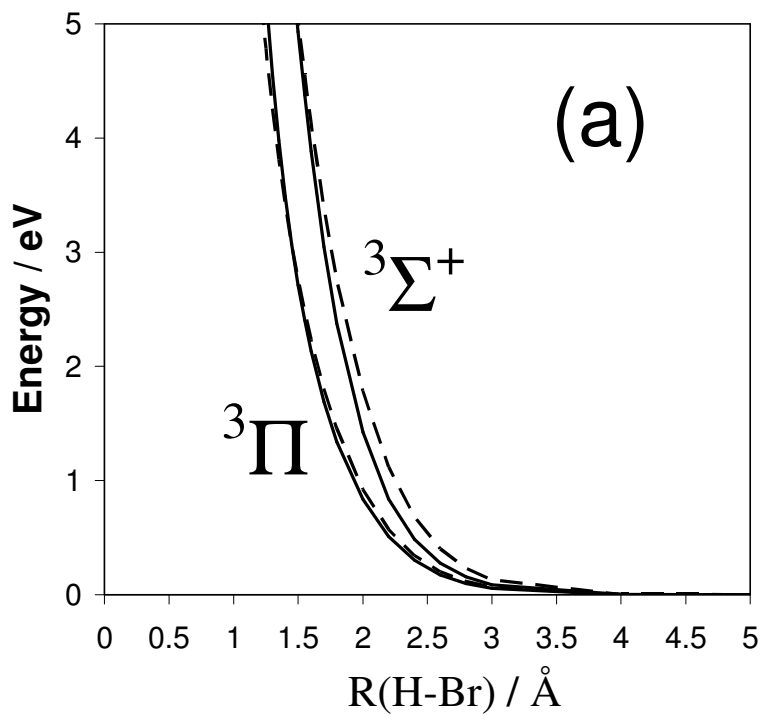


Figure 5

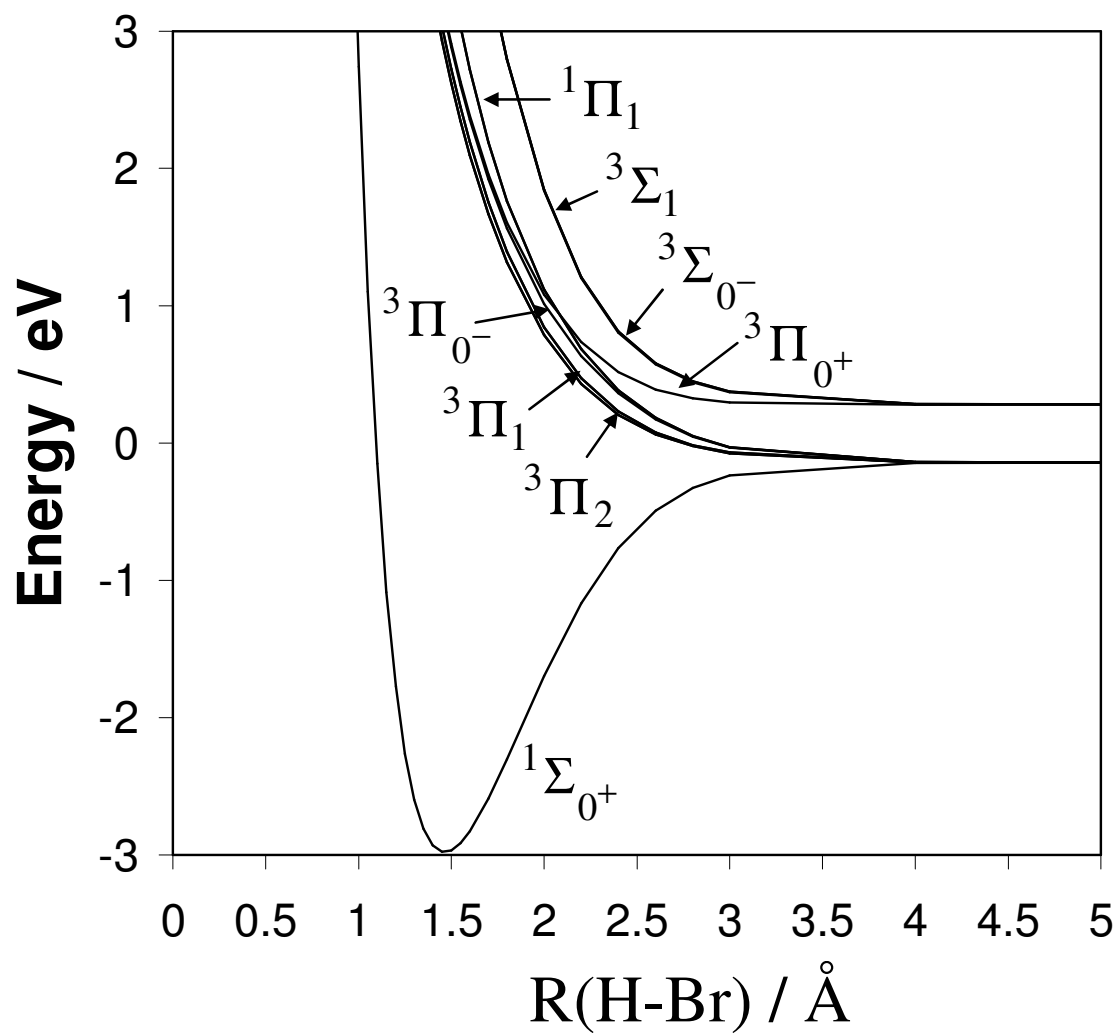


Figure 6

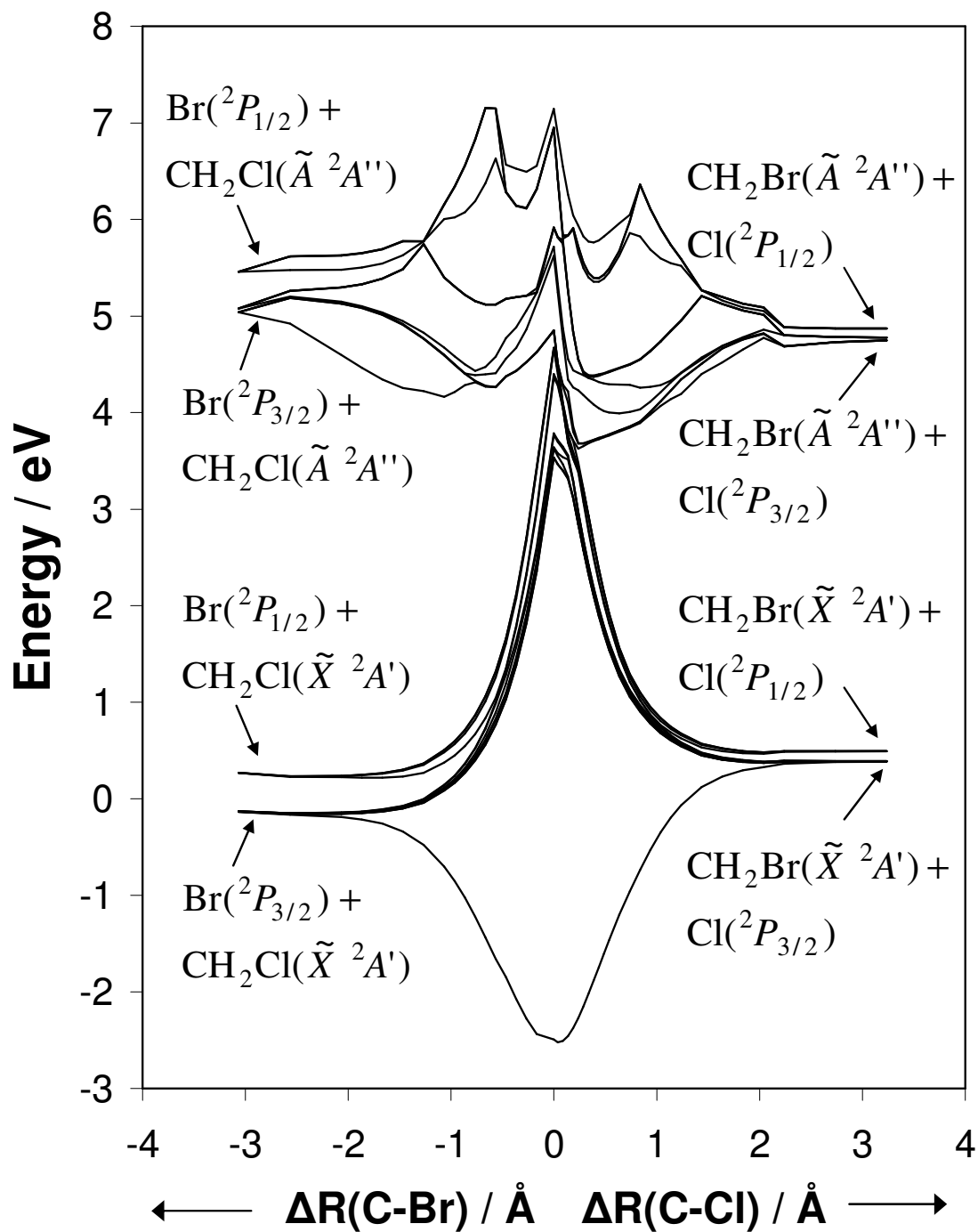


Figure 7

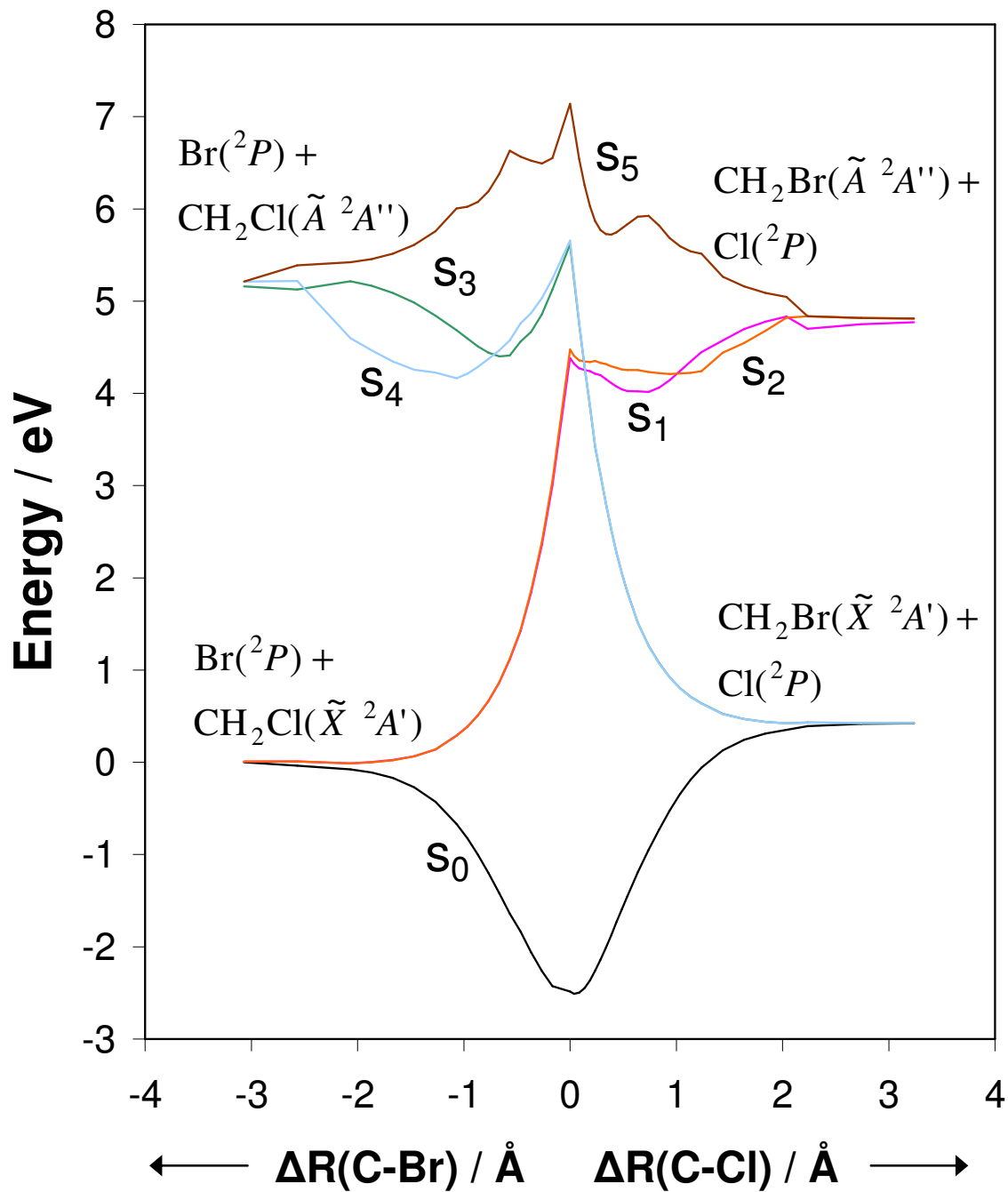
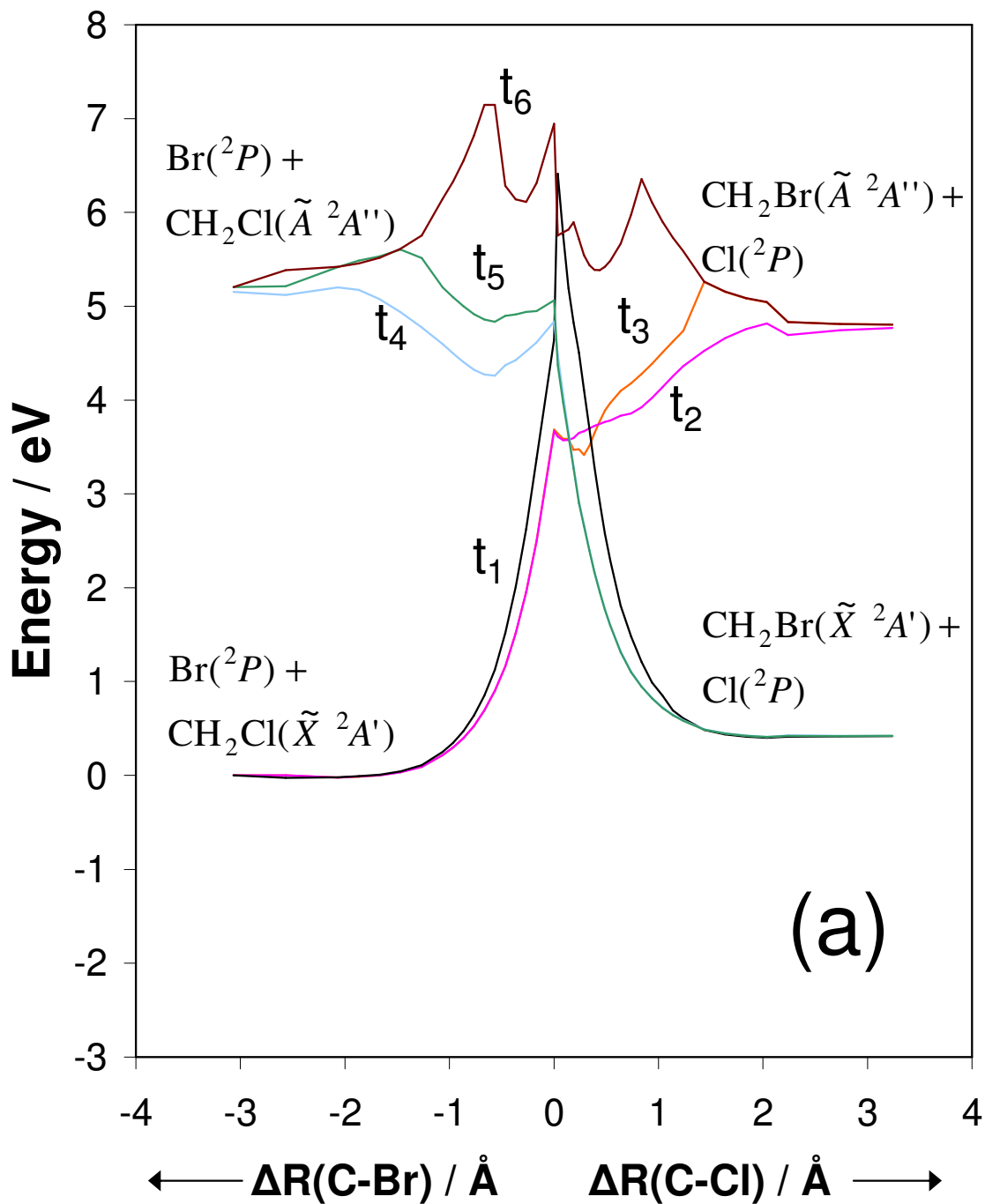


Figure 8



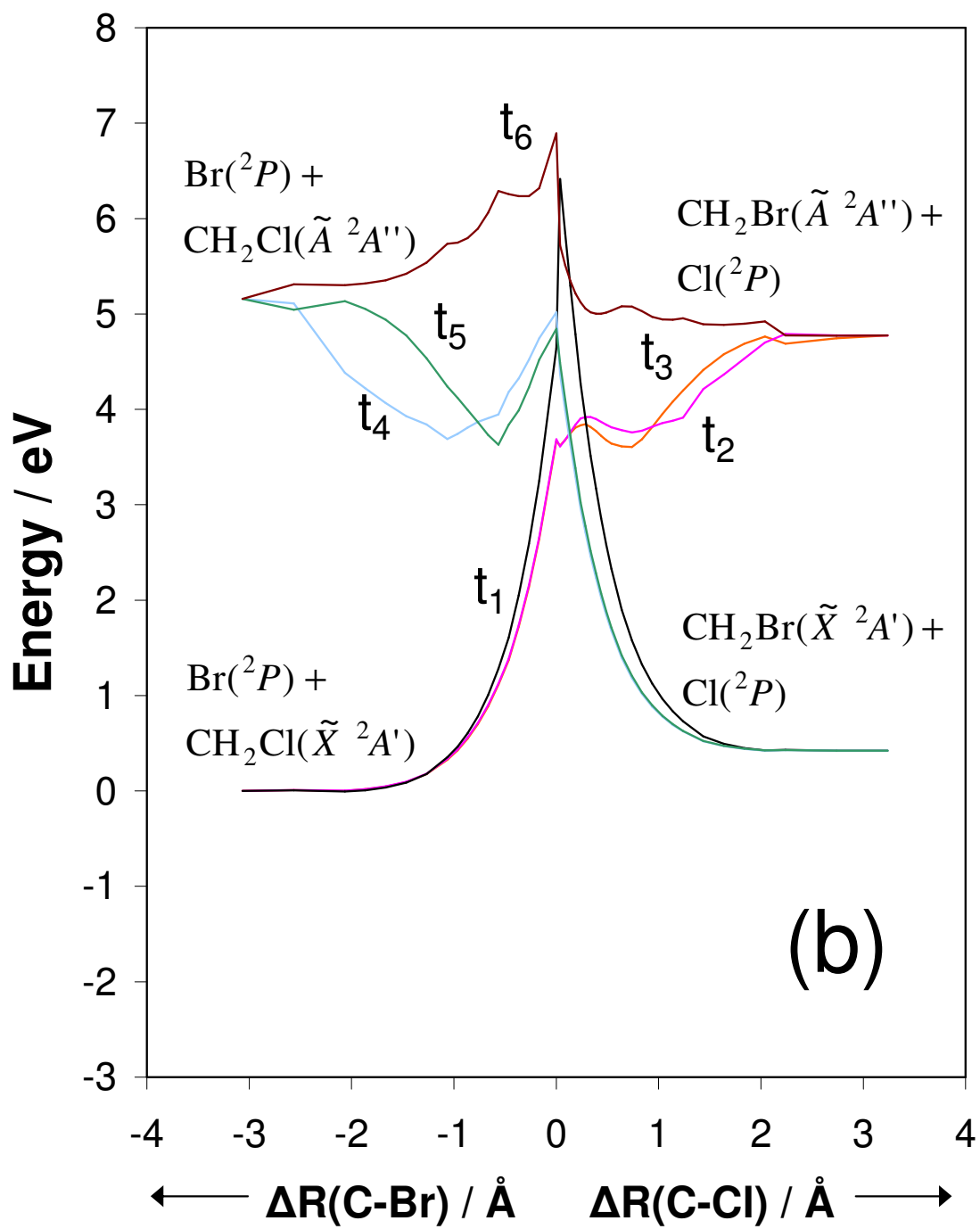


Figure 9

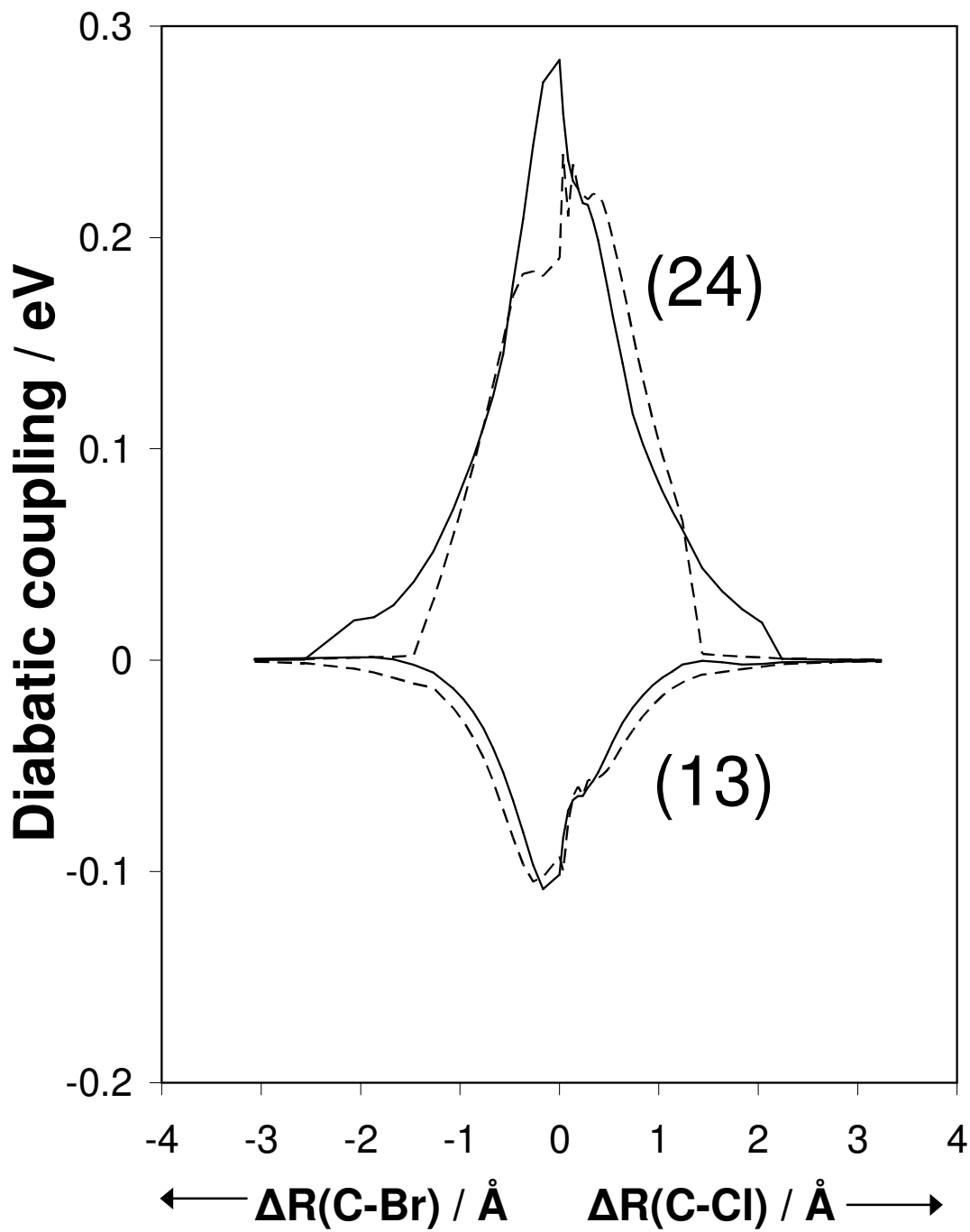


Figure 10

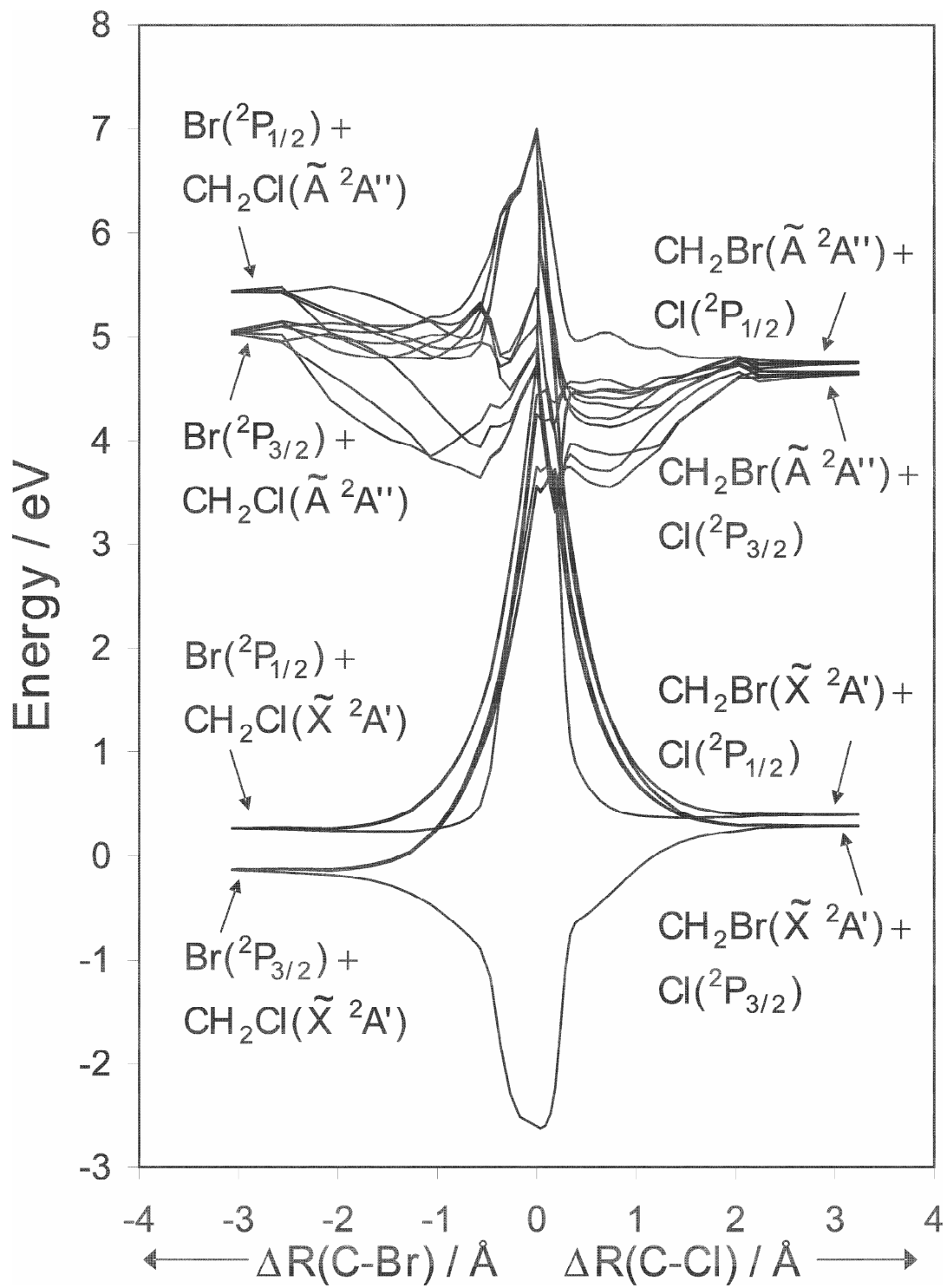


Figure 11

